THE DESIGN OF A MICROWAVE PHASED ARRAY HYPERTHERMIA SYSTEM

BY

TIMOTHY PAUL BENSON

B.S., University of Kansas, 1981

THESIS

Submitted in partial fulfillment of the requirements
for the degree of Master of Science in Electrical Engineering
in the Graduate College of the
University of Illinois at Urbana-Champaign, 1985

Urbana, Illinois

ACKNOWLEDGEMENTS

Thanks to the past and present staff of URI Therm-X for their help on this project, to Ron Boesch and Jay Loane who worked with me on this research, and to Harold Underwood and Brian Horowitz. Thanks also to Wanda Elliott for her help in typing and assembling this thesis and for her ability to find needed funding when accounts ran low. I am especially grateful to Professors Richard Magin and Clif Burdette for allowing me to work on this project and for their encouragement when things did not always go as planned. And a special thanks to my wife, JoEllen, for her never-ending support during the last year.

DEDICATION

This thesis is dedicated to my parents as an expression of thanks for their ever-present encouragement and support.

TABLE OF CONTENTS

CHAPTER 1

INTRODUCTION

1.1. LOCAL HYPERTHERMIA

Hyperthermia can be defined to be the elevation of temperatures in humans above 40°C (106°F) induced with therapeutic intent. This distinguishes it from normal fever (pyrexia) of up to 40°C and high fever (hyperpyrexia) which might occur as a result of sunstroke [1]. From this definition it can be noted that fever is internally produced temperature elevation while hyperthermia is externally induced temperature elevation. While hyperthermia has been used as a cancer therapy for over a hundred years, only now is equipment for physical hyperthermia emerging from the laboratory, being commercially produced, and gaining acceptance in the clinical arena. There exist many methods of hyperthermia treatment. Hyperthermia may be local, where only a small restricted area of the body is heated, regional, where an entire limb may be heated, or whole body. Techniques that have been used for production of hyperthermia include conduction through the skin (e.g., hot water bath), recirculation of externally heated blood, heated intravenous fluids, ultrasound, and electromagnetic (EM) coupling modalities. The EM modalities include inductive, capacitive, and UHF microwave radiation. These EM methods may be invasive or noninvasive depending on whether or not they require placement of the radiating element within the body.

1.2. Ultrasound and Microwave Hyperthermia

Most current research and development in hyperthermia instrumentation involve the use of ultrasound (acoustic) and microwave (electromagnetic) energy for heat induction [1]. Ultrasound is a useful method for inducing hyperthermia because of the ability to focus ultrasonic energy in small tissue volumes. This is due to the short wavelength in tissue which allows for sharp focusing with a small angle of divergence. Typically, the wavelength in soft tissue such as liver is about 1.5 mm at a frequency of 1 MHz. A disadvantage of using ultrasound is the problem of reflections from tissue interfaces, in particular, bone and air-filled cavities. At the muscle/bone interface up to thirty percent of the incident energy is reflected. Also, bone will absorb the ultrasound energy ten times more effectively than muscle [2]. Ultrasound cannot be used in the lung because of the many tissue/air boundaries.

Because of these potential problem areas, microwave techniques have been used for hyperthermia induction and have gained considerable interest recently as new equipment becomes available. Although tissue impedance mismatch and reflections also occur with microwave energy, the resulting problems are significantly reduced as compared to ultrasound. However, inherent shortcomings also exist for microwave energy. Most noteworthy is the inability to deposit significant power more than a few centimeters below the skin's surface. This is due to the attentuation of EM energy at microwave frequencies in muscle and skin. At 2450 MHz, for example, the depth of penetration is only 1.7 cm [3]. Another problem is that although the lower

microwave frequencies penetrate deeper in lossy tissue, the aperture dimensions of the applicator are usually relatively small compared to the wavelength, resulting in the energy being radiated in a divergent beam.

It is because of the disadvantages inherent in all hyperthermia modalities that no single modality is likely to replace the others. However, for a given clinical application, one method is usually preferable in a certain situation over the others. For instance, microwave hyperthermia would be better in treating tumors close to bone, or tumors in the lung or the brain. However, depending upon the depth of the tumor, it may not be possible to effectively treat a deep-seated tumor (e.g., liver) using microwave energy. In these cases, ultrasound methods are more appropriate. In the future, both types of systems will probably gain clinical acceptance and use.

1.3. A Controlled Microwave System

The purpose of this project and the subject of this thesis is the design and testing of a microwave phased array hyperthermia system. Chapter 2 will review previous and current microwave hyperthermia systems, and from these, highlight the advantages of the design described in this thesis. Chapter 3 discusses methods by which the phased array hyperthermia system could be implemented and presents the final design. Chapter 4 discusses the microwave phased array applicator and describes its design and testing. Chapter 5 identifies the other components used in the system and suggests approaches to be used for the optimal selection of each component. It also discusses a method

for control of all components in the system. The control aspect was to be the original focus of the research, but limited time and funding dictated that emphasis be placed on the applicator array, which is the key system component. Chapter 6 describes the test procedure and results of system integration testing. Finally, in Chapter 7, conclusions based on the research are described, and recommendations are made for the direction of future effort on this topic.

CHAPTER 2

A SURVEY OF HYPERTHERMIA TECHNIQUES EMPLOYING ELECTROMAGNETIC ENERGY

2.1. Capacitive Coupling

The coupling of electromagnetic (EM) energy into body tissue can be through one of three ways: capacitive, inductive, or radiative. Capacitive coupling is used with capacitor plates or contact electrodes to produce heating inside a patient. Most of this work has been done at either 13.56 or 27.12 MHz [4]. These two frequencies are approved for industrial, scientific, and medical work (ISM). The major problem associated with capacitive coupling and direct contact electrodes is that it results in heating patterns which are generally unpredictable. This is because the alternating current that is produced will follow the path of least resistance, perhaps even bypassing the intended target tissue. In addition, another problem occurs because the fat layer just beneath the skin is a highly resistive path which heats preferentially. This can, of course, be minimized by choosing a pathway where the fat layer is thin, or by using surface cooling on the skin. However, control of the heating pattern in deep-seated tissues is difficult using direct contact or capacitive coupling.

2.2. Inductive Coupling

The technique of using inductive coupling to produce hyperthermia was in use as early as 1893 by D'Arsonval [5]. He successfully heated an animal by placing it within a solenoid fed

by high frequency current. Another inductive coupling method involves flat contact applicators containing a pancake coil of several turns using the same ISM frequencies mentioned above. This overcomes the problem of overheating the fat layer due to high local E-field intensity in fatty tissues, but has little effect more than a few centimeters deep into high water content tissues such as muscle [6].

2.3. Radiative Coupling (Microwave)

The method of radiative coupling is by far the most widely used and researched of the EM methods. One way of using microwave radiation in hyperthermia is through invasive applicators, also known as interstitial antennas. This is done by placing a very small microwave antenna into a catheter which is inserted into the body where the radiation will affect the tumor. The obvious advantage is that the source of the radiation is placed at the point where the power is needed. The major disadvantages are those of patient discomfort and the need to often use multiple antennas to heat the tumor volume. Thus, in addition to the usual temperature monitoring probes that are inserted into the patient, there are radiating probes as well. This method, however, remains a viable option and is being used successfully for hyperthermic treatment (primarily brain and pelvic tumors) [7].

The alternative to invasive applicators is noninvasive applicators. This allows a patient to receive local hyperthermia treatment without having to place the applicator inside the body. When the noninvasive microwave applicator is used in contact with

the body, coupling efficiencies of 95% are possible [1]. Thus, virtually all of the incident power is transmitted into the body. Low water content tissues such as fat and bone absorb little microwave energy compared to skin and muscle. Even though the microwave energy passes through fatty tissues, it is severely attenuated in the high water content tissues such as muscle. As the frequency of the microwave radiation increases, the attenuation increases. At 2450 MHz, an approved ISM frequency, the power is reduced to 40% of the incident level at just 2 to 3 mm depth (assuming plane wave incidence and 1-cm fat thickness) [1].

Because of the problem of small penetration depth at 2450 MHz, most microwave hyperthermia work is being done at the next lower ISM frequency, 915 MHz, since the attenuation is less as the operating frequency is decreased. Figure 1 (all figures appear at the end of the text) shows absorbed power densities in skin, fat, and muscle at four ISM frequencies. As can be seen in Figure 1, regardless of the frequency that is chosen, the available power decreases rapidly because of absorption, divergence, and field fringing effects. As stated above, at microwave frequencies the skin absorbs a significant amount of energy, necessitating some method of surface cooling. One method being used to remove the excess surface heat is to circulate chilled distilled water through a bag placed between the applicator and the skin. Another method is to place several applicators above or around the tumor and energize them sequentially [8]. In this way, each applicator is contributing only a portion of the energy; thus, the skin beneath any one

applicator will not heat as much as if a single applicator were continuously radiating.

An improvement on the asynchronous, sequentially excited array is a synchronous phased array. If more than one applicator (either invasive or noninvasive) radiates energy toward a tumor such that their phases are identical at the intended focus, the E-field vectors from each of the applicators will add. Since power is proportional to the square of the voltage, the focus will receive power proportional to the square of the number of applicators. Because of the phasing requirement, this method requires a much more sophisticated control system than other methods. The synchronous microwave phased array approach is the one that was investigated in the course of this research and is described in the remaining chapters.

CHAPTER 3

SYSTEM DESIGN

3.1. Phasing Considerations

The proposed method for accomplishing the relative phase control of the microwave applicator in the hyperthermia system is known as conjugate phasing [9]. This technique is possible because of the property of reciprocity. A small radiating antenna is placed at the desired focal point, and the array is used to receive the signal. The amplitude and phase of the received signal at each array element are recorded. Then the phase conjugate is computed for each element and that element's phase control is set accordingly. A diagram describing such a system with four elements is shown in Figure 2.

Using the system in Figure 2, a small radiator is placed in the tumor at the position where the greatest power deposition is desired. The SPDT coaxial switch at the microwave source is switched to allow the probe to radiate. The array is used to receive the signal radiated by the probe. In this configuration, a portion the signal received at each element is sampled by the dual directional coupler located between the attenuator and radiating element. The signals received by each element are routed individually into the phase/amplitude comparator by means of Switch 4. The comparator will compare the received signal from an element with a portion of the source signal. The amplitude and phase difference for each element relative to the reference source is recorded.

After the phase and amplitude data for each channel have been obtained, the system is configured to transmit from the array into the tissue. The complex conjugate of the amplitude/phase value at each element is next computed. The position of Switch 1 is changed to direct the source signal to the array network. Switch 2 selects the input to the test channel of the comparator from one of the ports of the dual directional coupler; in this case, the forward coupled power is selected. Switch 3 is set to sample Channel 1. The phase shifter and attenuator are adjusted to match the desired conjugate amplitude/phase value for Element 1. This process is then repeated for the remaining elements. After the phase and amplitude of all elements are set, the computer can continually monitor the phase and amplitude and adjust these quantities in real time to effectively control the heated tissue volume.

One researcher has experienced a significant drawback to this method of conjugate phasing [10]. It is the problem of having insufficient signal strength for the comparator. The probe which is radiating in the tumor is a low power radiator--on the order of a few milliwatts total power. The signal is attenuated severely as it passes through lossy tissues such as muscle and skin, leaving little signal to be received at the array antenna elements. At this point an amplifier would likely be required to boost the received signal to a usable level. Otherwise, more power would be required at the probe, and it might as well be used as an invasive heating applicator itself. Another obvious drawback to the conjugate phasing method is the complexity and cost arising from many coaxial switches,

directional couplers, and the additional amplifier.

Because of the problems just mentioned, it was decided to approach the problem of phasing in a different manner. Essentially, to focus power at a particular point it is required to have all the incident E-fields add constructively at the desired focus. This is known as constructive interference and is achieved when the incident waves are in phase at a particular point. This result can be achieved by adjusting the phase of each channel until all the forward gain paths through the medium have the same phase value. A diagram of a system using this approach to phasing is shown in Figure 3. Using this method, a receiver probe is placed at the desired focal point in or around the tumor. Then a single element is turned on. This can be done with either a coaxial switch in each channel or by attenuating the other feed paths greatly with variable attenuators. The phase gain of the forward gain path of the element is recorded. This element is then turned off and the next one turned on. The variable phase shifter associated with the active element is used to set the forward phase gain of this element to match that of the first one. The same procedure is repeated for all of the remaining elements. Following this procedure, all elements can be activated, and constructive interference at the desired focus will result. This method is clearly simpler to implement than the conjugate phase method. It not only eliminates the need for a radiating probe. but also eliminates additional expensive couplers and coaxial switches. This approach also simplfiies the calculations needed to be done by the controller. Because of these factors, this second method for phase control is the one

that was implemented in this research.

3.2. High Power Options

It was assumed at the outset of this research that a power of at least 50 W per element (350 W minimum combined power) would be required in order to produce heating sufficient for hyperthermia at the tumor site. The assumption was based upon the results of computations of absorbed power required to raise the temperature of muscle tissue perfused at 3 ml/min/gram seven (7) degrees above normal *in vivo* tissue temperature. To produce this much power in a phased array system, two design approaches are possible. One approach is to use a single high power source at the front end of the system and divide the power among the system's channels such that each element will receive the required 50 W. The second approach uses a low power source divided among the channels, and then having an amplifier in each channel immediately before the antenna element. These two designs are shown in Figures 4a and 4b, respectively.

At first, using a single high power source (or a low power source and a separate large amplifier) appeared attractive because of the smaller number of components required. However, a source with power output around 500 - 1000 W at 1000 MHz is very costly (upwards of $10,000). While this may be practical in a research project, it is certainly prohibitive in a commercial product. Using a high power source also presents other drawbacks that are not immediately obvious. If variable attenuation is desired in each system channel, each attenuator would be required to dissipate a portion of the full power distributed to each

channel. This is grossly inefficient, results in undesirable heating and power dissipation, and is not cost effective. Another problem is the need for attenuators and phase shifters with high power handling capabilities. High power attenuators are considerably more expensive and more difficult to obtain than the readily available low power devices. The problems associated with high power phase shifters are worse than for attenuators. After searching through many catalogs and making numerous telephone inquiries, it was determined that continuously variable phase shifters which handle more than 2 W are not available. The solution to the phase shifter problem is discussed further in Section 5.3.

When using the system design with a low power source and multiple amplifiers, several advantages arise in addition to presenting solutions to the problems associated with the single high power source design. In the case of a failure of one amplifier, the system will function with only a slight degradation in performance. If the single high power source were to fail in that design, the system would be useless until repaired. Another advantage is that it might be possible to use variable gain amplifiers to control each channel's power output, thereby eliminating the need for variable attenuators. Thus, based on cost and the effect on other system components, it was decided to use a single low power source with small low cost amplifiers for each channel.

3.3. Final System Configuration

Based on the choice of phasing techniques and amplifying

scheme, the system as it is intended to be implemented is shown in Figure 5.

CHAPTER 4

MICROSTRIP APPLICATOR DESIGN

4.1. Array Configuration

As established previously, the proposed microwave hyperthermia system will use a phased array applicator. Although phased array technology is highly advanced in radar and communication systems, not much has been done in the field of heat therapy. The array to be used in this hyperthermia system differs in two ways from those arrays used in radar and communication [11]. First, the desired focal point of the hyperthermia applicator is only a few centimeters away, whereas the focal point is at an infinite distance for conventional arrays. Second, the hyperthermia applicator is required to be immersed in and radiate into very lossy media, whereas the conventional phased array radiates into unbounded, lossless free space. Because of these differences, the design problems are significant.

Fortunately, previous research done at the University of Illinois determined the optimal size and configuration for an efficient hyperthermia phased array applicator [12]. This study found that a hexagonal array consisting of elements in triangular lattices has some advantages over the standard rectangular or square spacing. Using the triangular lattice allows for wider element spacing within the array and for better control over grating lobes. Also shown was that an array with two outer rings with a total of 19 elements is most desirable (see Figure 6). Adding additional rings would not substantially increase the

focusing gain because of the greater attenuation of their E-field contribution at the focus due to longer path length through high loss medium. The final point of that study was the determination that the element-to-element spacing of 0.8 times the wavelength in the medium provided the best gain. In the current design, the only deviation that was made from these recommendations was the use of seven elements instead of 19. This was done to reduce the cost and to make it feasible to manually adjust the phase of the array elements.

It was decided for the purpose of this research to construct the phased array using microstrip (or patch) antenna techniques. A microstrip antenna is a very thin radiating device consisting of a slab of dielectric with a copper clad ground plane on one side and a patch of copper fed from the center coaxial lead on the opposite side [13]. A diagram of a simple microstrip antenna is shown in Figure 7. The use of a microstrip array has several advantages over a conventional array of dielectrically loaded waveguide elements. The microstrip or "patch" array would have the same face or aperture size but need only be a fraction of an inch thick as opposed to a waveguide array which must be at least several inches thick due to the required length of each waveguide element. A major disadvantage of a waveguide array requiring dielectric loading of each element is that the very high dielectric constant material required is available only as a power or as expensive, machined slabs. When used in power form, such material is difficult to work with and is not uniform in dielectric characteristics after being submerged in water. The microstrip array overcomes these problems. The material on which

the patch is constructed can be the same dielectric material used to load the waveguide, but in solid slab form.

4.2. Matching Process

The impedance characteristics of a microstrip antenna element are highly dependent on two factors: the shape of the element and the coaxial feed point [13]. Some guidance was available on how to construct a patch element for a fixed frequency radiating into air, but no handbook or papers were located detailing antennas designed to radiate into water. Therefore, it was decided to first build a printed circuit (PC) board microstrip element to radiate at 915 MHz into air. Using recommendations from members of the University of Illinois Electromagnetics Laboratory, a patch of dimensions 8.7 x 12.1 cm was made with the coaxial feed point centered along the long axis and 1.7 cm in from the side. Construction was on a piece of double sided copper-clad PC board. One entire side was covered with clear Scotch brand tape. On the other side, only the area of the desired patch was covered with tape. Then the board was immersed in a PC board etching solution for two hours. The result was the desired size patch on one side and a ground plane on the other. Next, a hole was drilled through the board at the desired coaxial feed point and a female SMA jack was soldered to the ground plane. The center conductor pin of the jack was soldered to the patch on the opposite side. The impedance was checked by viewing the S11 parameter on a network analyzer. It showed a relatively large magnitude reflection coefficient. This needed to be lowered by making the feed point closer to the edge

of the patch. This meant retaping both sides of the board except for the thin strip which was to be removed. After removal, the reflection coefficient was improved; it is shown in Figure 8 as plotted on the Smith chart. This antenna was used as a guide to aid in the design of a patch antenna for operating in a high dielectric medium, such as water.

The next step was to construct a microstrip antenna designed to radiate into water. The first attempt was to scale down the dimensions of the patch antenna designed for use in air by the square root of the dielectric constant of the new medium. The dielectric constant of water is about 80, therefore the new patch would be scaled by a factor of about nine. The idea of scaling the patch did not take into effect the properties of the substrate or the physically large size of the coaxial feed relative to the patch, and therefore did not provide an adequate impedance match.

For this patch element and all subsequent ones, a dual channel Hewlett Packard 438A power meter was used to make reflected power measurements. The configuration for the reflected power test is shown in Figure 9. A 3 dB hybrid coupler and two power sensors were used to make simultaneous forward and reflected power measurements. Figure 9 also details how the attenuation in the cable leading from the hybrid coupler to the patch and the losses in the hybrid itself were used to compute an offset for each channel in the power meter. Once these offsets were entered in the power meter, it would compute the forward and reflected power at the patch using the offsets, divide the reflected power by the forward power and display it as a

percentage of forward power.

At this point it was decided not to continue using double sided copper-clad PC board. The iterations of taping, etching for two hours, and then removing the tape were too time-consuming. For this new smaller PC board microstrip antenna, single sided PC board was used and the patch was made using copper foil tape (3M Company, Minneapolis, MN). This tape comes in rolls one inch wide by 18 yards in length with an adhesive on the reverse side similar to regular household tape. As a result, trimming a patch becomes much simpler. When a patch needs to be made smaller, all that is needed is to slice off a narrow strip of the foil tape using a sharp knife.

The scaled down dimensions of the air radiating patch did not result in a good impedance match to the 50 ohm coaxial feedline. Many different sizes and shapes of patches with varied feed points were examined. It was noted that feeding the patch near one edge resulted in less reflected power than other feed points examined. Once this was completed, resonant patch lengths were found (between 22 and 26 millimeters) which resulted in dramatic decreases in reflected power. When this resonant length was achieved, a decrease in patch width would further decrease the reflected power until the patch was narrow to the extent of potentially impairing its power handling capability. Using this process and exercising care, a patch was made that reflected only five to ten percent of the incident power. This process was repeated for the remaining six elements. A diagram of the array with its dimensions is shown in Figure 10. Pictures of the array are shown in Figure 11a. Using the field scanner system

described in Chapter 6, principal plane (E-field and H-field) cuts as well as a raster scan were made of the pattern of a single element (Figures 12-14).

As can be seen in Figure 12, the x-axis principal plane cut shows a symmetrical pattern. The y-axis (Figure 13) cut is not symmetric. Because of the irregular pattern in the y-axis, it was decided to produce a microstrip array on a slab of ceramic which has dielectric properties closer to that of water. The new substrate is known as MCT-85 (Trans-Tech, Gaithersburg, MD). MCT-85 is a ceramic dielectric material made of Magnesium Calcium Titanate (MCT). It has a dielectric constant of approximately 85 with a dielectric loss tangent of less than 0.001. Because this material is extremely brittle, great care had to be exercised in drilling through it. A single hole was drilled in the middle of the slab for a test patch using a diamond tipped core drill. Since there was no copper backing on this material, copper foil tape was placed on one side to create the ground plane. A female SMA jack was soldered to the foil and to the patch on the opposite side (Figure 11b). Since the copper was not clad to the ceramic, the jack was only as stable as the ability of the foil adhesive to hold it in place. Therefore, care had to be taken not to exert much force on the SMA jack.

The matching procedure for the new substrate was the same as that used for the PC board patch array. As found previously, there existed a resonant length which provided the lowest reflected power level. For this array the minimum reflected power occurred at a length of 16 millimeters. Again, the percentage of power reflected decreased as the width of the patch

was decreased. For the MCT-85 substrate, good impedance matches were obtained for practical widths of individual patches. It was found that once the resonant length had been determined, the reflected power was a linear function of the patch width (see Figure 15). This allowed for a width to be predicted given a desired reflection percentage. For this center element and the six succeeding ones, a reflected power percentage of from six to ten percent was achieved using a patch width equal to approximately seven millimeters (see photograph in Figure 11a). With this design it was anticipated that a more symmetric and uniform field pattern would result in the y-axis (E-plane). This was indeed the case, as is shown in Figures 16-18.

CHAPTER 5

SYSTEM COMPONENTS

5.1. Microwave Source

In Section 3.2 the rationale for using a low power source was presented. For purposes of driving the amplifiers selected for this research, about 15 dBm, or 32 mW, was needed for each channel. For a seven channel system, this would require 221 mW exclusive of the insertion loss through the power dividers, phase shifters, attenuators, and miscellaneous cable and connector reflections and loss. A fairly reasonable source power for the system would be about 1 W. This presented a problem, however, since most low power microwave sources are less than 10 mW. It was clear that a source would need to be coupled with a low power amplifier to boost the signal to the required strength. One source under consideration was a highly stable, mechanically tuneable, 100 mW source from Engelmann Company (Model HFE). This oscillator was purchased with a specified center frequency of 915 MHz. The 100 mW power output level permitted performance of focusing tests without the need for individual channel amplifiers. A 100 mW input power level would provide a signal which could still be detected at a focus several centimeters deep in the lossy medium. As it turned out, this oscillator was used without amplification in all tests because of the lack of availablity of seven separate amplifiers and because the available signal strength was adequate without additional amplification. In Figure 19, the supply voltage versus output power curve is shown for this oscillator.

5.2. Attenuators

The next component found in each channel (moving from source to antenna element) in the system block diagram, is a variable attenuator. The purpose of the attenuator is to adjust the power delivered by each element. It is desirable to have equal power output from each element, but because of variations in component isolation loss, amplifier gain and antenna radiation efficiency, a network of equally divided elements may not produce equal power at each element. Therefore, some type of control over each channel is required. A variable attenuator is a good way to achieve this control, but depending on the amplifier used in the system, separate attenuators for each channel may not be necessary. If a fixed gain amplifier is used having a power output dependent on the input power, an attenuator can be effectively used in front of the amplifier to control the output power. If, however, the amplifier produces a nearly constant output power regardless of the input power within a defined operational range, an in-line attenuator in front of the amplifier would have little or no effect. This type of fixed output power amplifier was one of two amplifiers being considered for use in the system. However, the gain of this type of fixed output amplifier could be adjusted with a variable DC power supply. Because a variable attenuator would be simpler to control, and less expensive than variable power supplies, it was decided to use the fixed gain amplifier mentioned above. Additional criteria for choosing the amplifiers used in the system are discussed in Section 5.4.

Variable attenuators are available in several forms from

many manufacturers. One type of attenuator is an analog voltage controlled PIN diode attenuator (Figure 20a). With this attenuator, a control voltage determines the amount of attenuation the device provides. A second type is the digitally programmable attenuator. One way to make this device is to use an analog voltage controlled attenuator with a D/A (digital to analog) convertor section attached. A second way is to build the device in cells, with each cell controlled by a digital input, and each cell having twice the attenuation of the previous cell (Figure 20b). This type of attenuator is the easiest to incorporate into a digitally controlled system and is also the least expensive. An eight bit programmable attenuator with the least significant bit being 0.1 dB would yield an attenuation range of 0.1 to 25.5 dB which corresponds to a range of approximately 2.3% to 99.3% power attenuation. An eight bit attenuator of the type just described can be readily obtained for less than $200.

5.3. Phase Shifters

Specifying and selecting programmable phase shifters for the hyperthermia system proved to be a major problem. At the beginning of the project it appeared that digitally programmable phase shifters available from several manufacturers would be the obvious and simple solution. Upon closer scrutiny it soon became clear that these devices were not what was needed. First of all, these phase shifters are very low power devices; most of them specify a maximum input power of less than 10 dBm (10 mW). Finally, these devices have insertion losses ranging from 3 dB to

6 dB. With the low input power and high insertion loss, there would not be enough power remaining to drive the amplifier. In addition to this problem, the lowest price found for a five bit phase shifter, which would give phase shift resolution to 11.5 degrees, was around $1500. This was more than the expected price of the amplifier. Finally, availability of this device was poor. Clearly, it was not an option that could be seriously considered.

An alternative involved construction of an analog phase shifter. By driving a small current into the IF port of a mixer, a signal fed into the RF port will undergo a phase shift at the LO port (Figure 21a). Tests were performed to evaluate this method and results of the test are shown in Figure 21b as a graph of input current versus phase shift. As can be seen from the graph, the slope is extremely steep and would require precise control of a very small driving current. The major drawback, however, is the large isolation between the RF and LO ports. The isolation measured during test of the Watkins-Johnson M1-A mixer was between 26 and 28 dB for all input power levels. Using the 26 dB figure, this means that only one quarter of one percent of the power input at the RF port is available at the LO port for feeding to the amplifier. Thus, to obtain the roughly 20 mW input required at the amplifier, about 12 W would be needed at the input port of this phase shifter. An input power of 12 W would exceed the maximum input power handling capability of the mixer, thus rendering the approach impossible.

A third possible solution involved using a 3 dB hybrid coupler to implement a variable phase shifter [14]. When the coupled ports of a 3 dB coupler are identically loaded, all input

power is transferred to the output port with no loss. In addition there will be a phase shift of 90° plus the angle of the reflection coefficient of the loaded ports. Several types of phase varying loads can be applied to the coupled ports including a varactor, a series inductor-varactor, and a parallel inductor-varactor. It has been shown that the parallel inductor-varactor will provide the greatest phase variation with the least capacitance variation [14]. The capacitance variation is produced by varying the reverse bias voltage across the varactor. Since the phase shift is dependent on a voltage, the phase shift can be controlled by a computer using a D/A converter. The phase shift generated can be shown to be

$$\angle\Gamma = 2\tan^{-1}\left(\frac{\omega L}{Z_o(\omega^2 LC-1)}\right) - 180^\circ$$

As the reverse bias voltage across the varactor is changed, its capacitance changes, thus changing the phase of the reflection coefficient. A graph plotting reverse bias voltage versus phase shift is shown in Figure 22. This plot assumes a specific tuning ratio, unswept angle, median capacitance, and inductance. Detailed information on this design is available in reference [14].

An advantage of this design is that it allows for precise phase changes over the entire 360° range. It is also possible to build this design using inexpensive, readily available components. The 3 dB hybrid couplers are also capable of handling high power and, as used in this application, would contribute little insertion loss.

5.4. Amplifiers

As previously noted, two models of amplifiers were being considered for use in the hyperthermia system. Both are capable of producing about 50 W of power to the antenna element. The smaller, less expensive unit is the North Hills PA-101. A 7 W version of this amplifier was loaned to us by the manufacturer for evaluation. A graph of amplifier gain (Figure 23) phase versus frequency and input power (Figure 24), and a graph of amplitude versus frequency and input power (Figure 25) for the North Hills amplifier are shown. The North Hills PA-101 is a Class C type amplifier and thus does not provide a phase-stable output. However, this problem can be corrected by the control system. Since phase feedback is provided to the system, the nonflat phase gain response of the amplifier can be compensated for, once the output power level of each channel is set by the programmable attenuators.

A second amplifier under consideration was the Avantek AWP-900. This is a physically large Class A amplifier which requires between 0.75 and 1.6 W input power. Output power is not dependent upon the input power but rather on the supply voltage. Thus, as discussed in Section 5.2, attenuators would not be needed for use with this amplifier. Since either amplifier could be used in the system, it was decided to incorporate the North Hills model into the design mainly because of the cost differential and lower power dissipation of Class C operation. The Avantek AWP-900 was priced at over $2000 while the North Hills 45W model was roughly half that price. Because of the adapability of the control system, a Class A amplifier was

unnecessary. Specifications for these amplifiers are shown in Table 1 (all tables appear at the end of the text).

5.5. Control System

The control system for the microwave phased array could be run by a microprocessor, possibly an Intel 8031 microcontroller or a similar device. This device would have its own control program and would receive commands from a host computer. Those commands would instruct the system to configure itself for a new focal point, to increase or decrease power, or to start or stop. Through a set of parallel output ports and latches, the microcontroller would output controls to the phase shifters, attenuators, and the coaxial switches required to route signals to the phase-amplitude comparator. Through parallel input ports, it would read the phase and amplitude difference between signals at the comparator.

The phase-amplitude comparator itself has not been well defined. It could consist simply of a vector voltmeter or network analyzer with analog phase and amplitude recorder outputs. This would be an extremely expensive route to pursue. The system diagram shows the test and reference signals being mixed down to lower frequencies for input to a phase/amplitude comparator. This is definitely an area for further investigation, since the ability to compare the phase of two microwave signals is key to the proper setting of the phase relationships among the array elements for focusing.

A flow chart of the microcontroller sequence is shown in Figure 26. It consists of two main branches: one to set the

elements in phase for focusing, and the other to monitor phases and power levels during operation.

CHAPTER 6

SYSTEM INTEGRATION AND TEST

6.1. Test Equipment

The heart of the system test apparatus used to determine prototype array performance is a three-axis computer controlled field scanner and data aquisition system [15]. A block diagram of the scanner is shown in Figure 27. An Apple IIe computer with a custom interface card is used to control three stepper motors which position a probe in three axes and to input the probe signal. The computer can be instructed to do a single axis scan in any of the three axes or to perform a raster scan in the x and y axes. The single axis scans are immediately displayed on the screen and can be printed on a graphics printer. The two axis raster scan data can not be displayed and are instead saved on diskette for later use.

Another element of the system test hardware is a Hewlett-Packard 438A Dual Channel Power Meter. As mentioned previously, this power meter can use separate offsets for each channel, calculate ratios, and display in dBm, watts, or percentage. The power meter has a zero to one volt range analog output which follows the range selected on the display. This analog output is connected to the amplifier circuitry of the scanner system for automated data recording. To be used with the power meter, the amplifier circuitry needed minor modifications since it was designed to accept a low level ac signal from an ultrasound hydrophone probe. The power meter output is zero to one volt dc, and the interface circuit in the Apple IIe has a

zero to ten volt dc range. Fortunately, the last amplifier stage on the amplifier circuit card was a simple noninverting operational amplifier with a gain adjustable from one to ten. All that was needed was to add a switch and a female BNC jack. The modified amplifier circuit is shown in Figure 28.

A considerable amount of time was spent modifying the controlling software of the scanner system. This was to be expected as it was the first use of the scanner for recording microwave antenna pattern data. Several software bugs found during the course of making field plots were subsequently worked out. A major drawback to the existing scanner system was the limited control of software execution. The flow of the main control algorithm was sequentially driven, which meant there was no convenient way to do a quick scan unless the peak had previously been found, a very time-consuming task. The flow diagram of the control software as it originally existed is in Figure 29 followed by the replacement menu driven controller in Figure 30. The menu allows the user to execute any of the six major functions or subroutines of the scanner without having to follow a restrictive flow sequence. This allowed for much more flexibility in using the scanner as a tool and subsequently saved considerable time and effort.

Another large undertaking was the writing of data reduction software. This software was in the form of a three-dimensional plotting program that would produce three-dimensional plots of x - y axis raster scans. Raster scan data are always saved to diskette, and no programs existed to make use of this form of data. The data are stored on diskette as 12-bit positive binary

values. The plotting program first opens and reads the data header file which contains information describing the data stored in the binary data files. The information includes the type of scan, center scan coordinates, step size, and scan ranges. The user is prompted for plot labeling information, and the program then opens the data file and plots the data. The program was somewhat more difficult than expected due to the need for hidden line algorithms and the peculiarities of the Hewlett-Packard 7470A plotter. A listing of the raster scan plot program is presented in Appendix. This raster scan program was twice modified to produce programs which would plot single axis, 2-D scans. These listings are not provided since they are simplified versions of the 3-D plot program.

6.2. Test Configuration and Description

As several components were not available for use on this project, testing was confined to verifying the power deposition increase of a phased array over a single element. Missing from the system block diagram were attenuators and amplifiers. The tests were done using only the single 100 mW microwave source. Since programmable phase shifters were not available, line stretchers were used to produce a phase shift. A block diagram of the test setup is shown in Figure 31a. A photograph of the test bench is shown in Figure 31b.

To make a scan of a single element, the 100 mW source is connected to the element feed cable with a 30 dB coupler in-line. The channel A power meter probe is connected to the coupled output, and the channel B probe is connected to the cable of the

receiver probe. Channel B is displayed on the power meter and thus is fed to the scanner amplifier circuit via the power meter's analog output. Scans may now be made in any of the three axes desired, and the patterns immediately printed or saved to diskette storage for later plotting. All that is required to make pattern plots of an array is to insert a feed network consisting of power dividers following the coupler.

The following procedure is used to set the phases of a seven element array. In place of the channel A and B power meter sensors, the reference and test channels of a PRD model 2020 vector voltmeter are connected at the 30 dB coupler and the receiver probe, respectively. The receiver probe is positioned at the desired focus. The element 1 feed cable is connected to the through port of the 30 dB coupler. The phase is read from the vector voltmeter and recorded. This is done for all seven elements. A value is now picked for the target phase of all seven elements. If two or more elements' phases are close to each other, the remaining elements can be set at this value. Phase values of elements are adjusted by adding line stretchers or cable extenders to the feed cable. A cable extender adds about five to ten degrees of phase, whereas a line stretcher is adjustable between zero and 25 degrees plus the shift inherent to the length of the line stretcher. Once all phase values are close enough (within ten degrees of the desired phase), the cables, including stretchers and extenders, are connected to the feed network and the feed network to the coupler (Figure 32).

6.3. Test Results

Results of phasing the two microstrip arrays were encouraging but did not yield the expected gain [12]. Principal plane cuts and a three-dimensional raster scan of the PC board patch array antenna (x = 0 cm, y = 0 cm, z = 4 cm) are shown in Figures 33-35. The coordinate system for the pattern measurements is shown in Figure 36. It is seen that the irregular E-plane pattern (y-axis) observed for a single element is still present when the array is focused. Comparing these patterns with those in Figures 12-14, a gain increase of 163% was experienced along with a 24% reduction in the 3 dB beamwidth. (The half power beamwidth data are summarized in Table 2.) The 163% gain figure translates into a 2 dB gain. The gain increase and beamwidth decrease are expected results but not quite as good as the design criteria.

As discussed in Section 4.2, it is because of the irregular y-axis pattern and the desire to use a substrate for the array with a dielectric constant closer to that of the test medium that an array was built using the MCT-85 substrate material. First, this array was phased to focus along the principal axis at (x = 0, y = 0, z = 4). Principal plane cuts and a raster scan are shown in Figures 37-39 for comparison against the single element patterns in Figures 16-18. The comparisons show a gain increase of 153% or 1.9 dB. The 3 dB spot size decreased 11% from 9.25 cm^2 to 10.5 cm^2.

The MCT-85 substrate array was again phased, this time to focus off axis at (x = -1.5, y = 3, z = 4). Principal plane cuts and a raster scan for this pattern are shown in Figures 40-42.

Again, these should be compared to the single element patterns in Figures 16-18. In this case the gain was only 2% or 0.1 dB, and the spot size decrease was only 8%. It can be seen from the plots that the beam did focus off axis as desired. Unfortunately, no more attempts at focusing could be made because of borrowed equipment that needed to be returned.

CHAPTER 7

CONCLUSIONS AND RECOMMENDATIONS

7.1. Conclusions

The results presented in Section 6.3 were encouraging and support the concept of using applicators incorporating a phased array of elements to provide greater power deposition and smaller beam size in the desired heating region than is possible with a single antenna element being fed the same input power. However, the increase in power delivered by the array compared to the divergent beam applicator was on the order of 2 dB versus the theoretical value of greater than 6 dB. This research shows that the use of phased array technology in clinical hyperthermia is possible and that it possesses several advantages: first, more power is deposited at the tumor site than with single element applicators; and second, the input power is distributed over a much larger skin surface area resulting in less incident power density, thereby reducing the potential of burns and patient discomfort.

Several possibilities exist to explain the somewhat low power gain figures. The patch antennas are not perfectly matched and coupling effects were seen. When all seven elements are connected, the 6 - 10% reflected power from each patch is reflected into the power dividers where they may add in phase. These multiple reflections may be adversely affecting the elements' radiation efficiency. In addition, since variable attenuators were not used, the power radiated from each element was slightly different. Ideally, one would like equal

contribution from each element at the focus, and as this was not possible, may have contributed to the lower gain.

One part of the project that was not demonstrated was computer control of the system. Since programmable phase shifters were not available, it was not possible to implement the proposed automated control system. However, with the digitally controlled components incorporated into the system, a microcomputer would be capable of initially setting the phases of each channel and adjusting them during treatment. Such adjustment would be dependent upon feedback from a temperature monitoring system and a central control algorithm.

7.2. Recommendation for Future Work

Although this research has provided a basis for an interactive hyperthermia therapy system using microwave phased array techniques, additional work is needed to implement the complete computer-controlled system concept. The most immediate need is for variable phase shifters. As discussed in Section 5.3, phase shifters can be made inexpensively using hybrid couplers and this design should be pursued. A second need is for a phase/amplitude comparator. The lack of these two devices was the major stumbling block to practical implementation of the total system. Their absence necessitated use of line stretchers and SMA extenders for phase shifters and a vector voltmeter that would not provide consistent measurements. With these two needs met, a total computer-controlled phased array system with feedback would be feasible to implement.

Another area of needed research and expertise is that of the

microstrip antenna design. The designs built during the course of this research were done by trial and error with only basic theoretical guidance. The shape of the patches that was finally used in focusing performance tests was not what was expected (a rectangular patch with an interior feed point). More work needs to be performed to determine the effect of various substrates, patch geometry, feed point location, and the medium in which the antenna is operating upon overall antenna efficiency.

As can be seen from the results, this research has proved the feasibility of using a microwave phased array applicator in a hyperthermia system and shown that it has several advantages over a single element applicator. The next logical step in this research is the development and demonstration of a totally automated phased array microwave system building upon the methods and results obtained from this work.

TABLES

Table 1

Amplifier Specifications

	Avantek AWP-900	North Hills PA-101
Input Power	0.75 - 1.6 W	4 - 26 mW
Output Power	12 - 45 W	0 - 45 W
VSWR (max)	1.5:1	2.0:1
Supply Voltage	12.5 VDC	19 - 30 VDC
Supply Current	6 A	10.2 A
Volume	1683 cm^3	58 cm^3
Weight	3.5 Kg	0.3 Kg

Table 2

Half Powers Beamwidths (HPBW) of Single Elements and Phased Array Applicators

	Single Element		Phased Array	
	H-plane	E-plane	H-plane	E-plane
PC board array focused at (0,0,4)	7.4	*	5.6	*
MCT-85 array focused at (0,0,4)	3.8	3.1	3.1	3.4
MCT-85 array focused at (-1.5,0,4)	3.8	3.1	3.2	3.4

* Irregular pattern in E-plane did not permit calculation of HPBW.

FIGURES

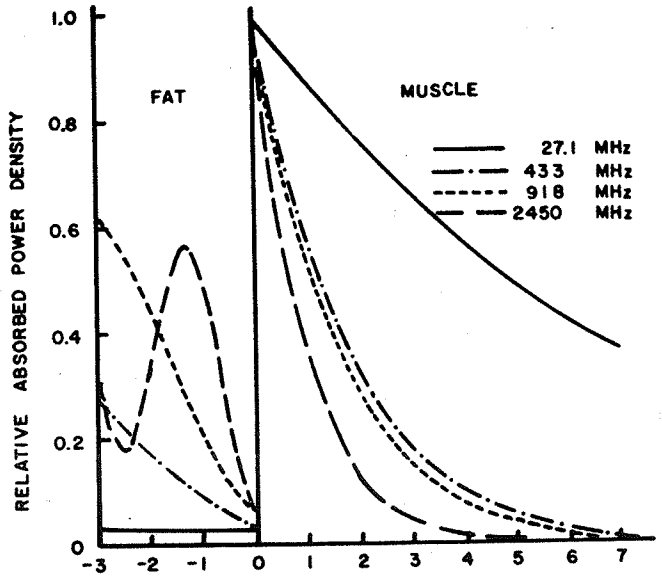

(a)

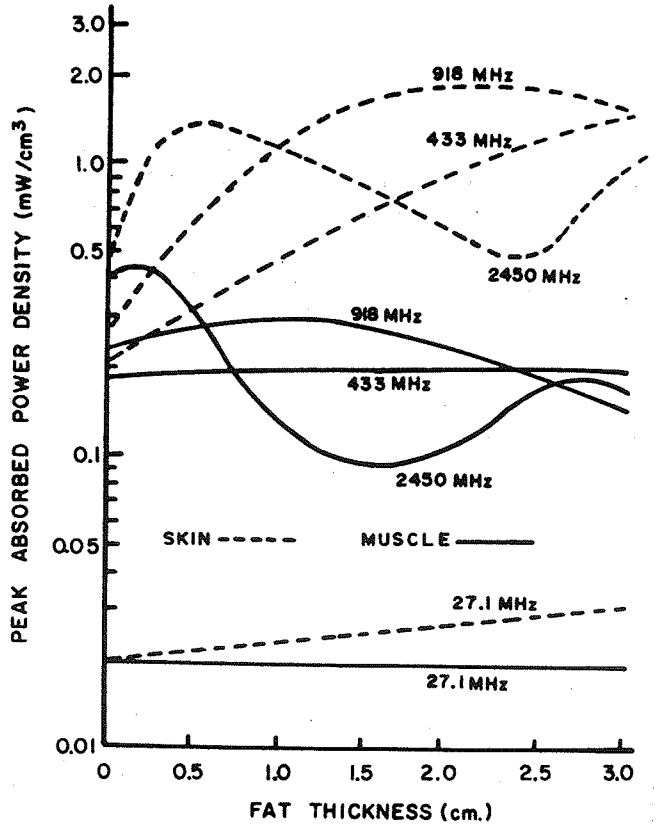

(b)

Figure 1. (a) Relative absorbed power density patterns in fat and muscle layers and (b) peak absorbed power density patterns in skin and muscle as a function of fat thickness [16].

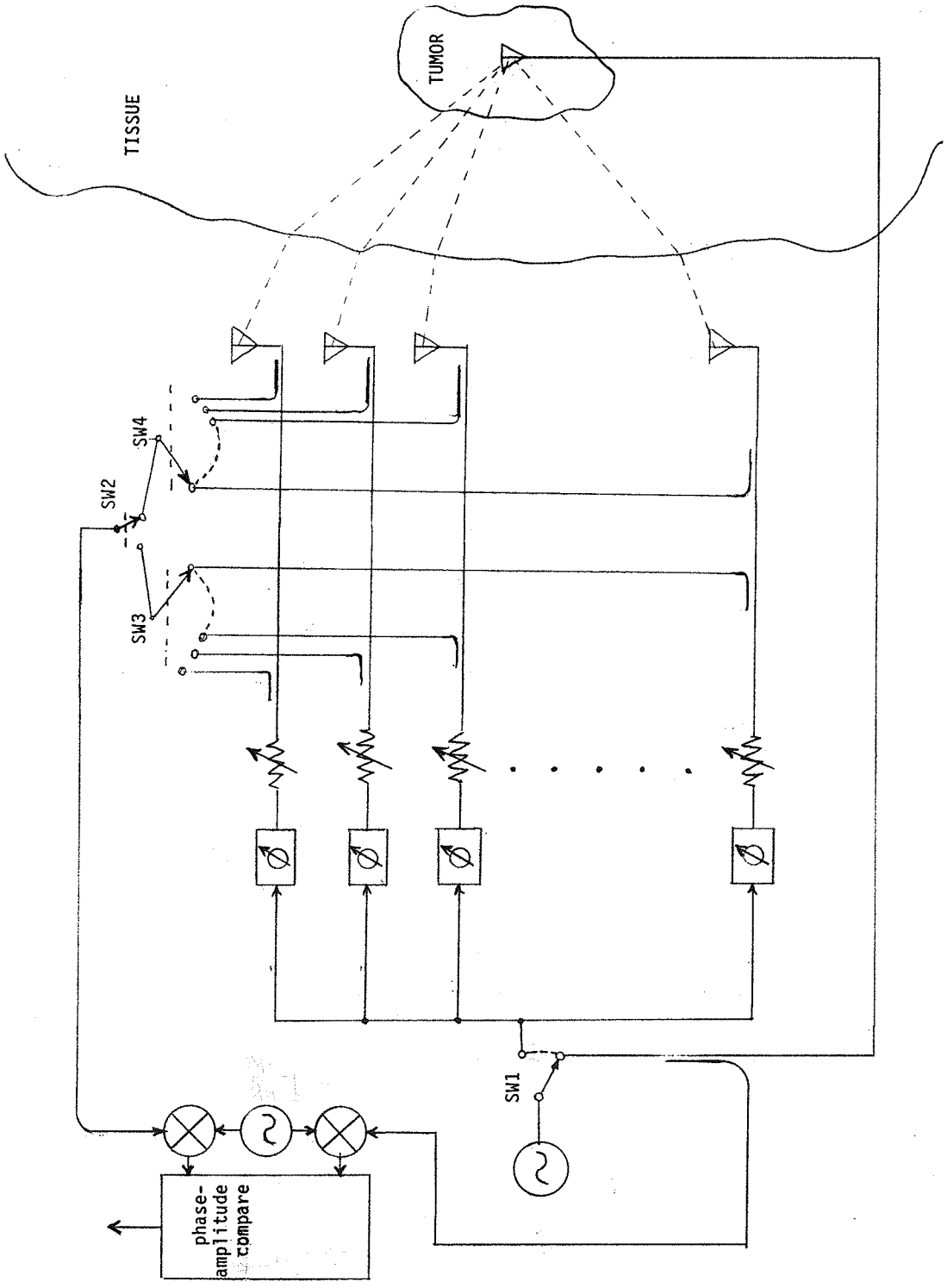

Figure 2. Conjugate phase method block diagram.

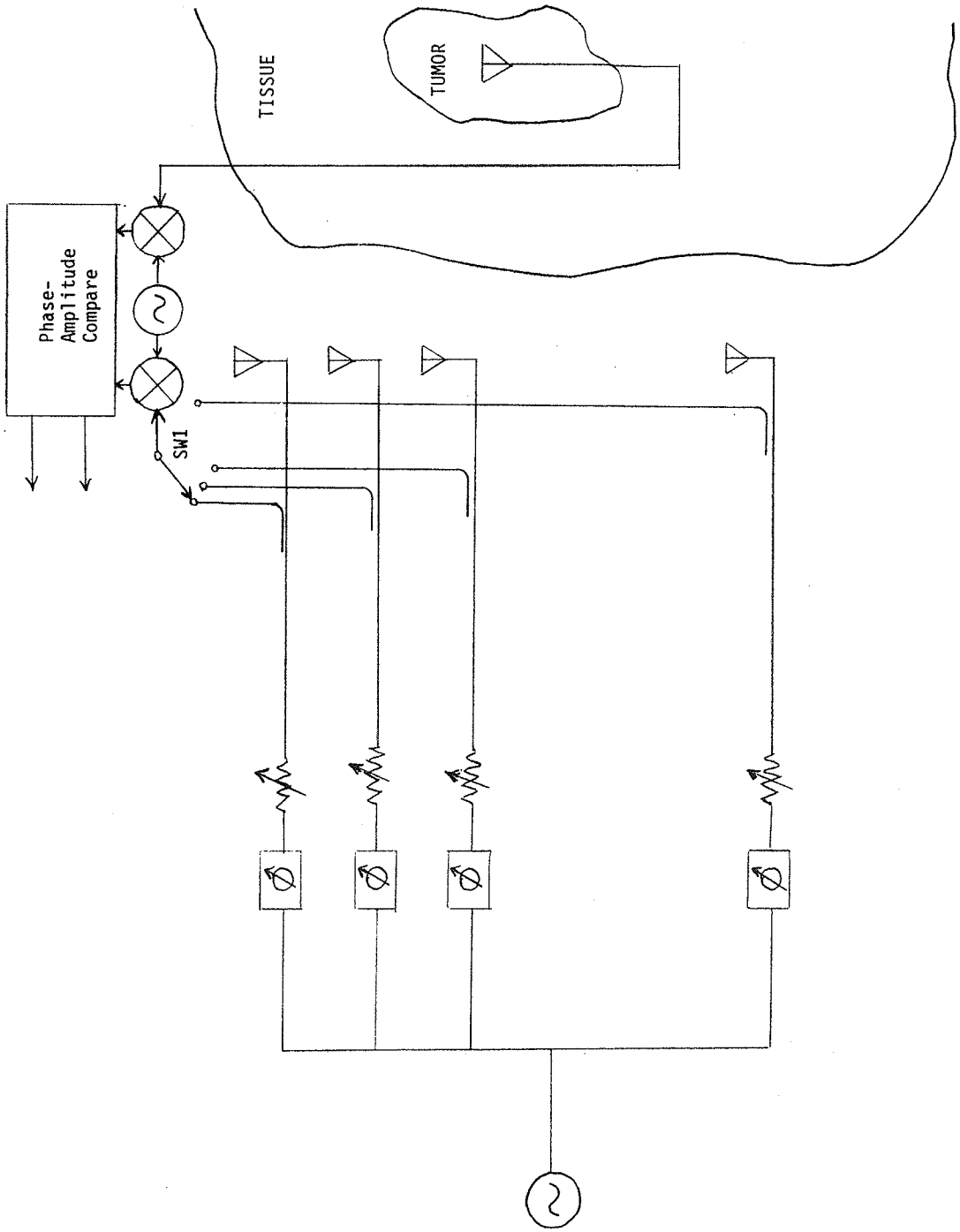

Figure 3. Phase matching method block diagram.

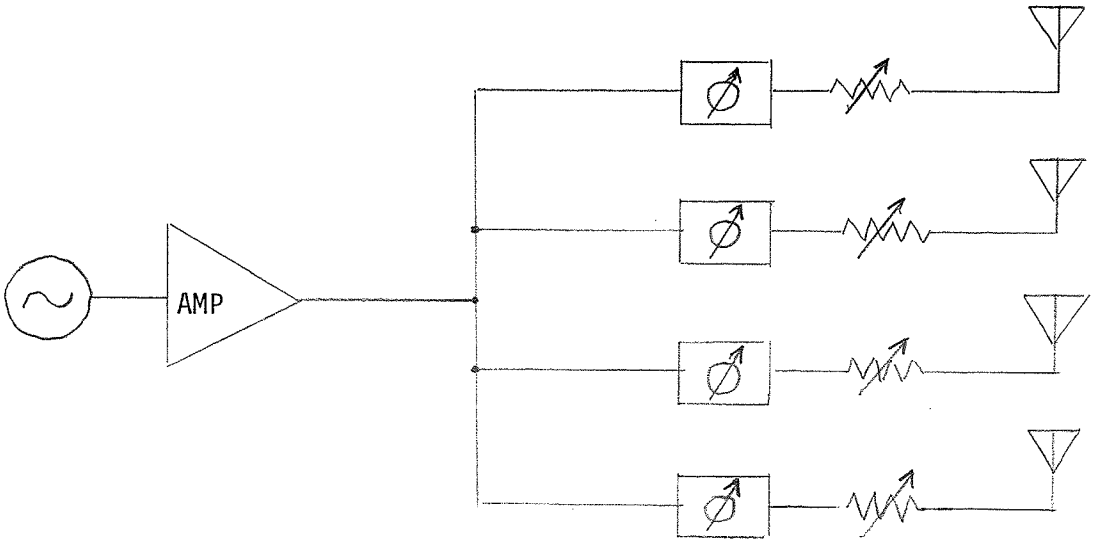

(a)

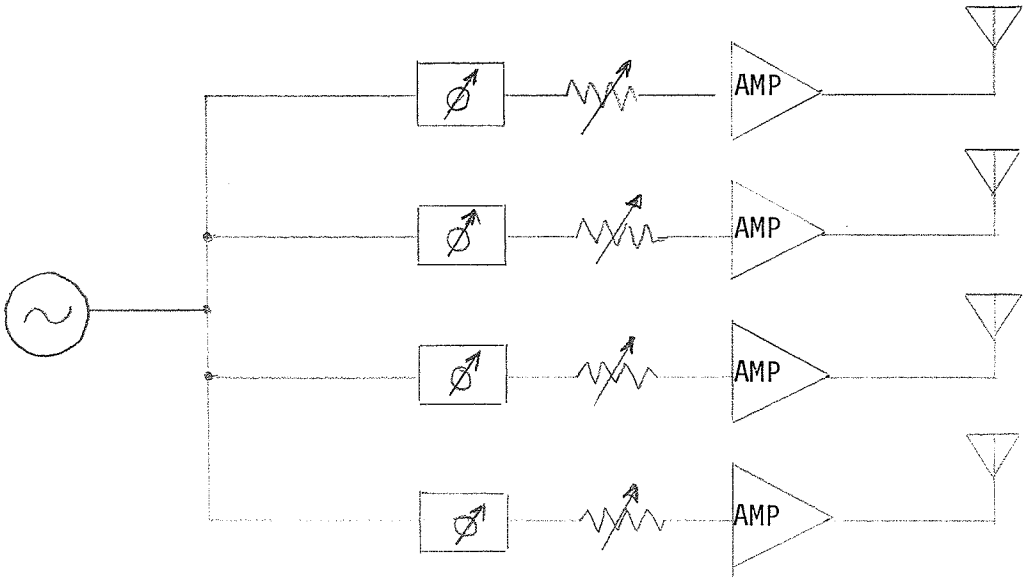

(b)

Figure 4. (a) High power source block diagram and (b) low power source block diagram.

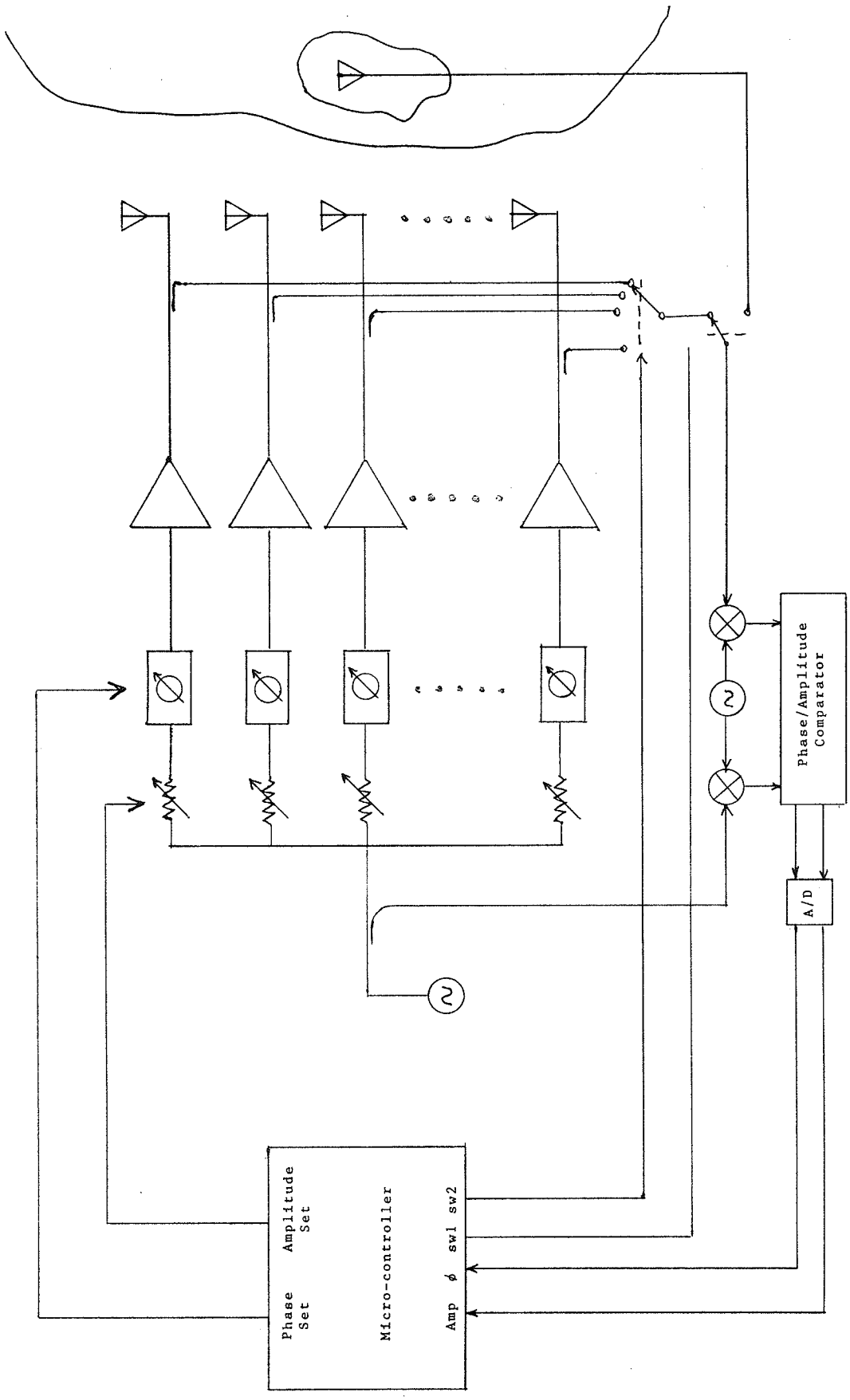

Figure 5. Microwave phased array hyperthermia system block diagram.

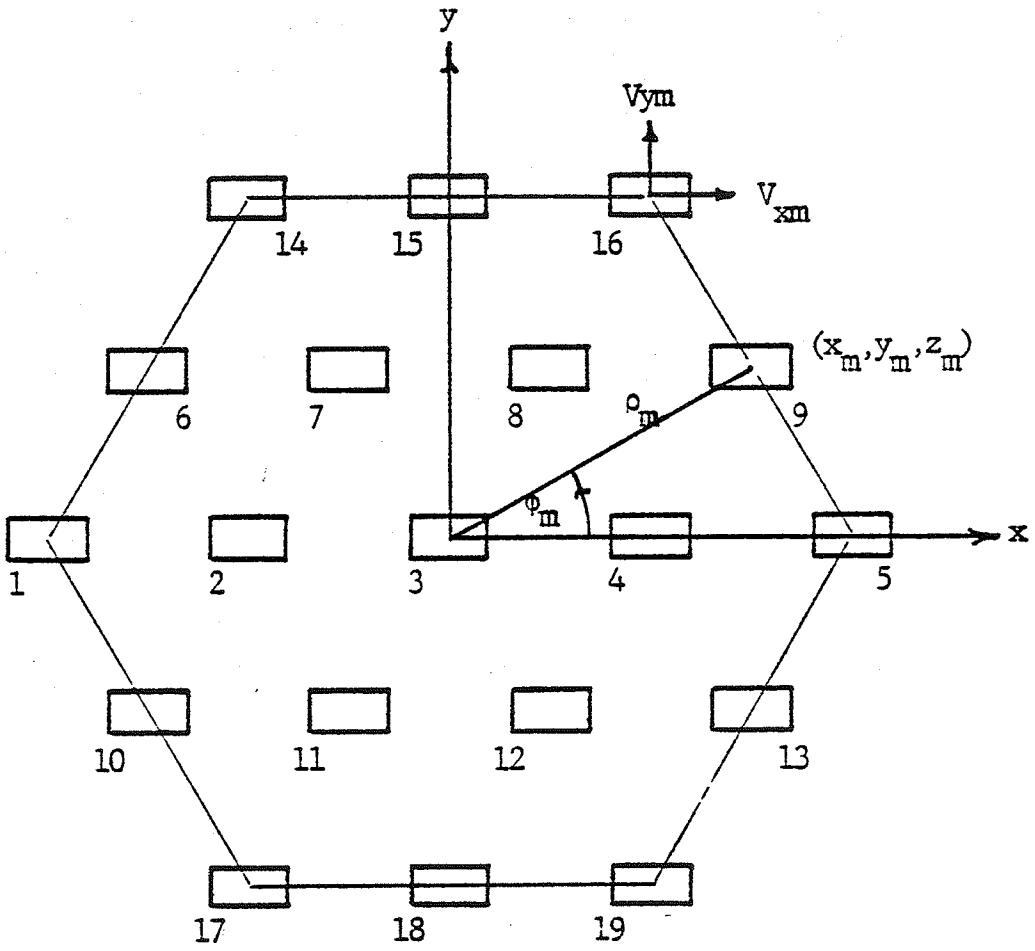

Figure 6. Geometry of 19 element hexagonal array.

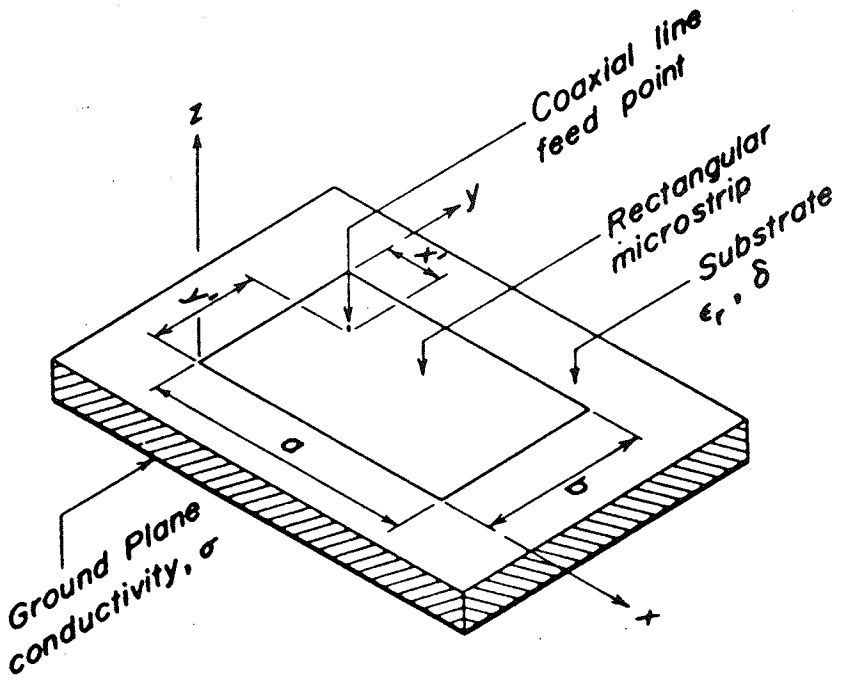

Figure 7. Microstrip antenna construction [13].

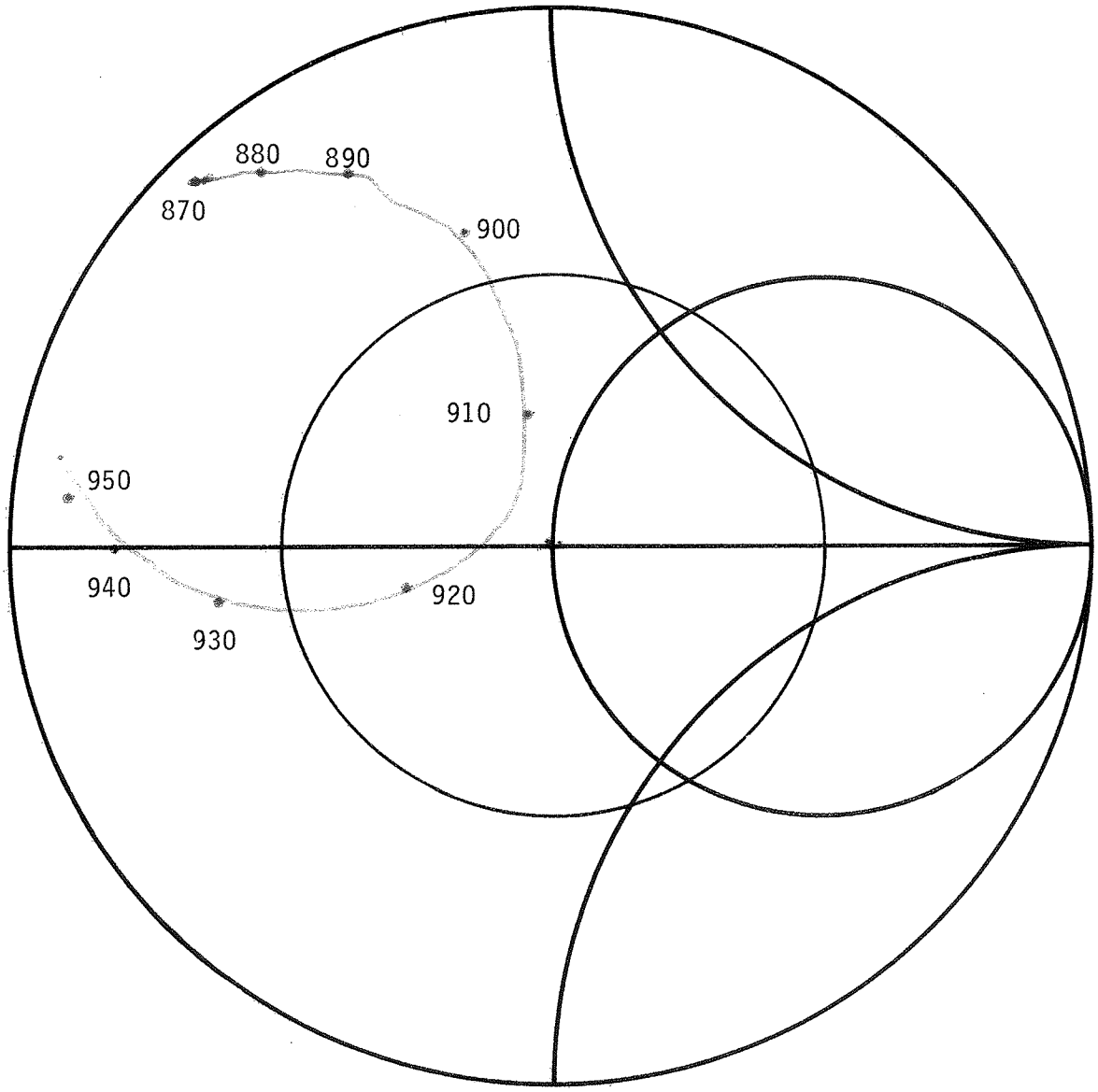

Figure 8. Smith chart plot of S_{11} coefficient of microstrip patch radiating into air.

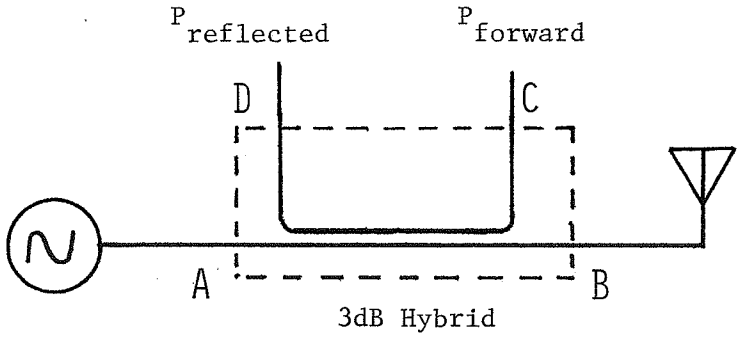

LOCATION	LOSS
Port A to Port C	3.12 dB
Port B to Port D	3.14 dB
3' of R/G142 coax	0.36 dB

Offset for power meter channel A ($P_{forward}$) = 3.12 - 0.36 = 2.76 dB

Offset for power meter channel B ($P_{reflected}$) = 3.14 + 0.36 = 3.50 dB

Figure 9. Measurement of reflected power.

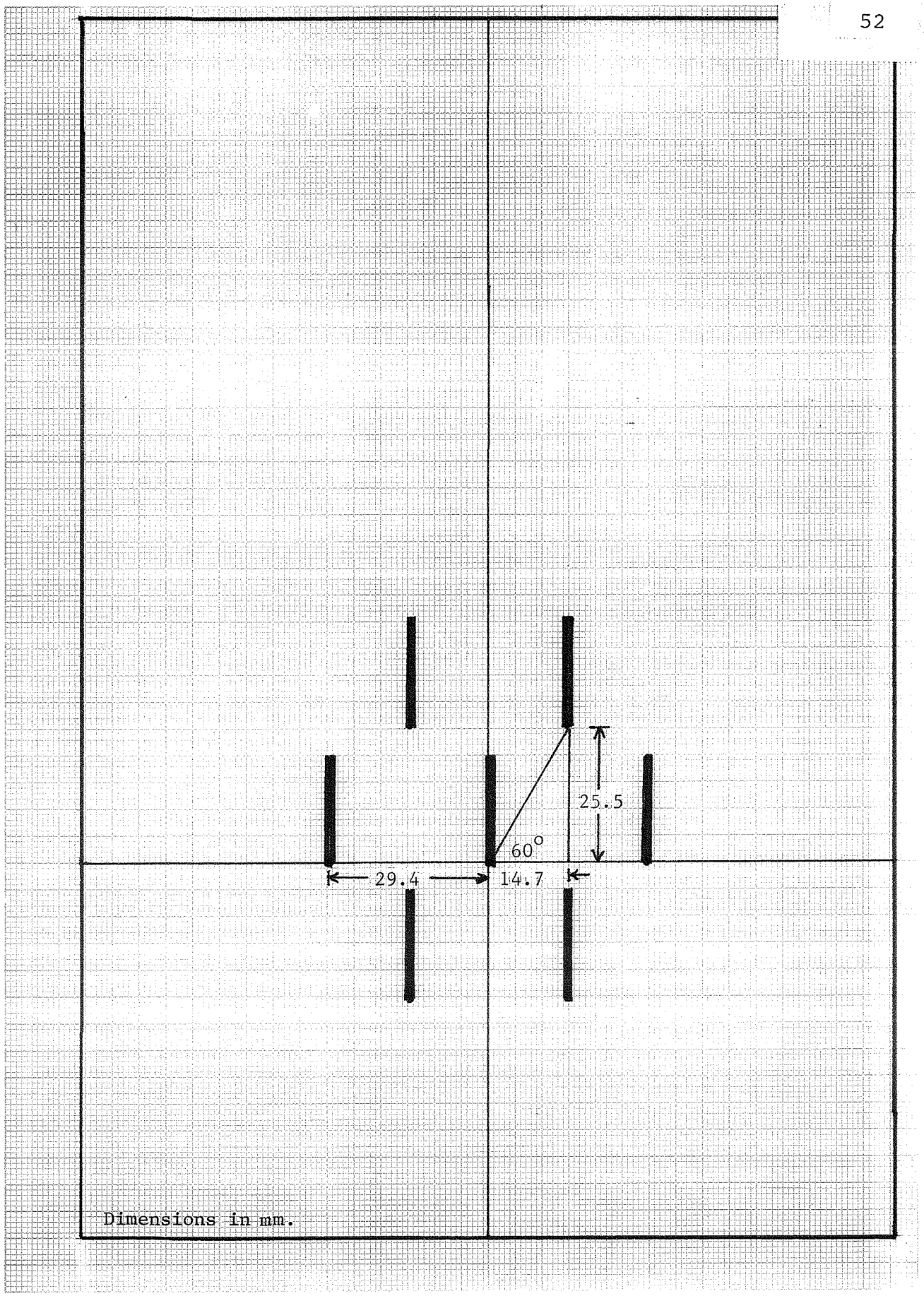

Figure 10. Geometry of seven element PC board microstrip array.

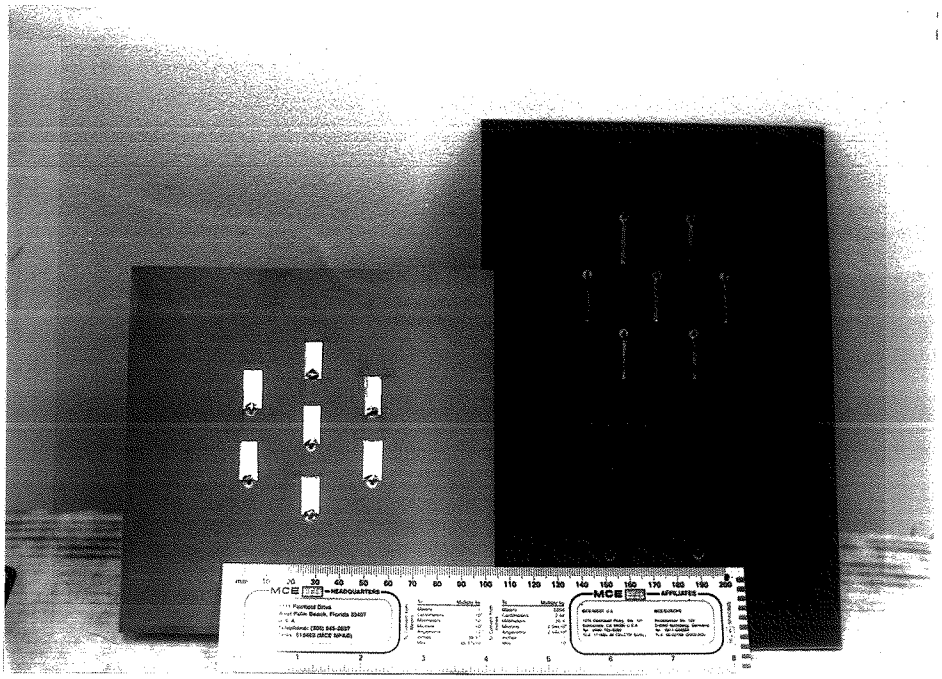

(a)

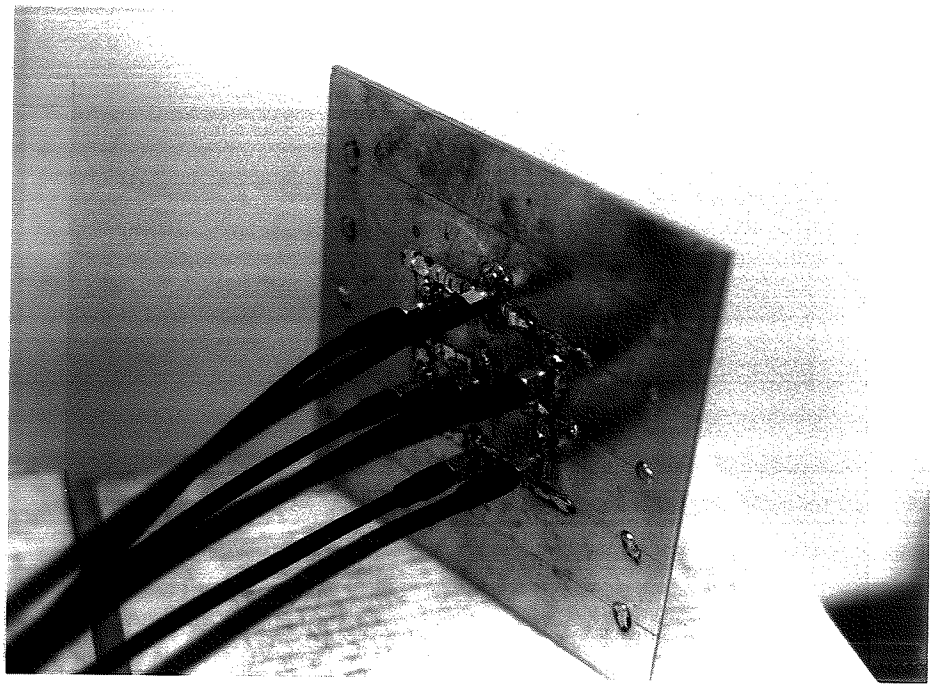

(b)

Figure 11. (a) MCT-85 (left) and PC board (right) microstrip arrays and (b) photo detailing feed connections on MCT-85 array.

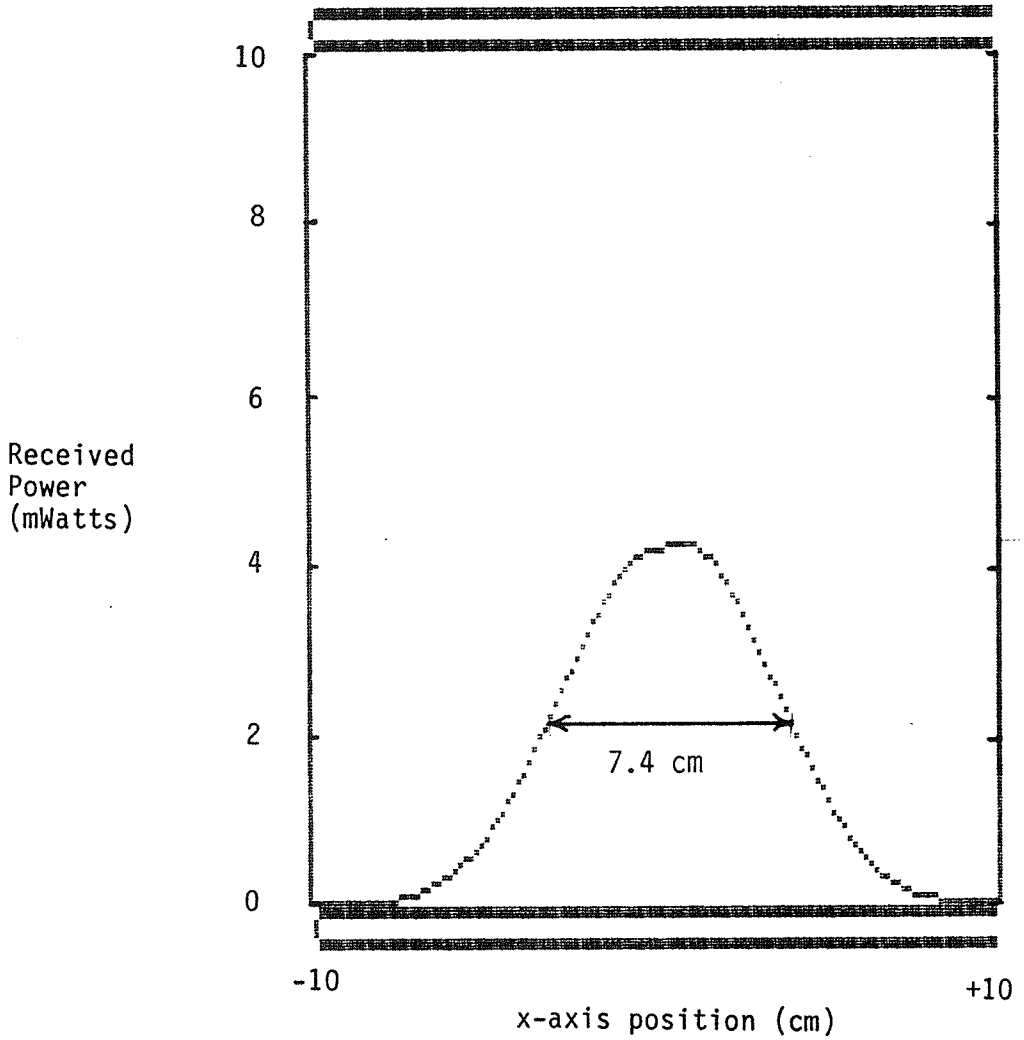

Figure 12. H-plane principal axis pattern plot of a single PC board microstrip element.

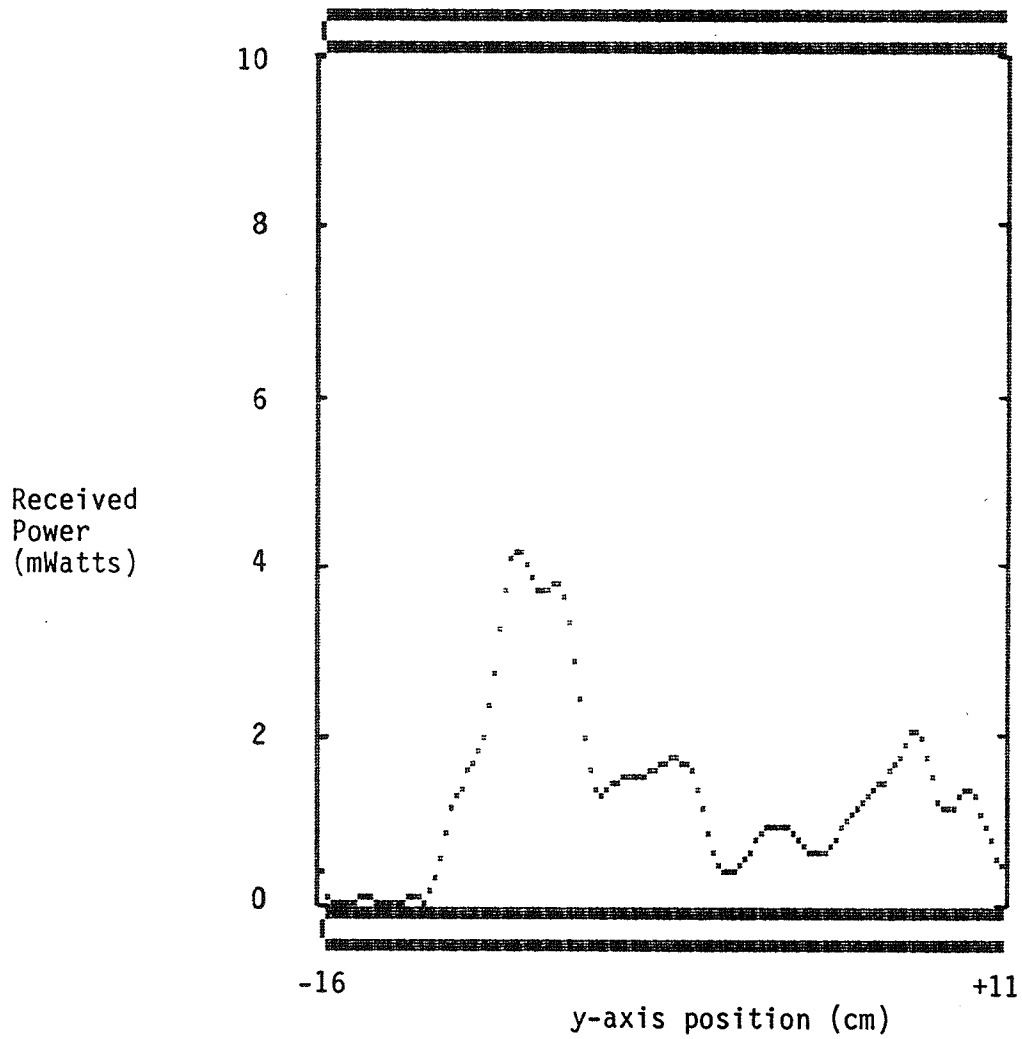

Figure 13. E-plane principal axis pattern plot of a single PC board microstrip element.

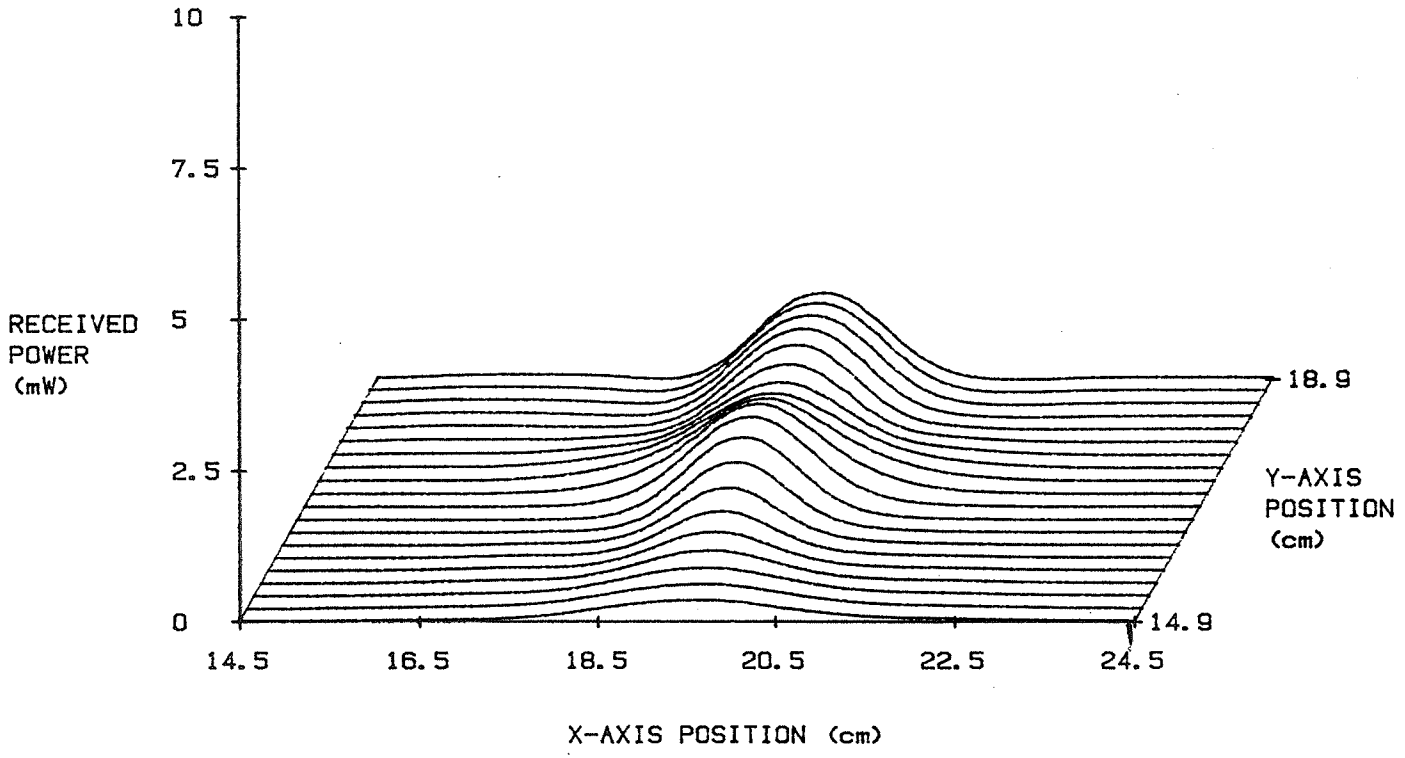

Figure 14. Contour pattern plot of a single PC board microstrip element.

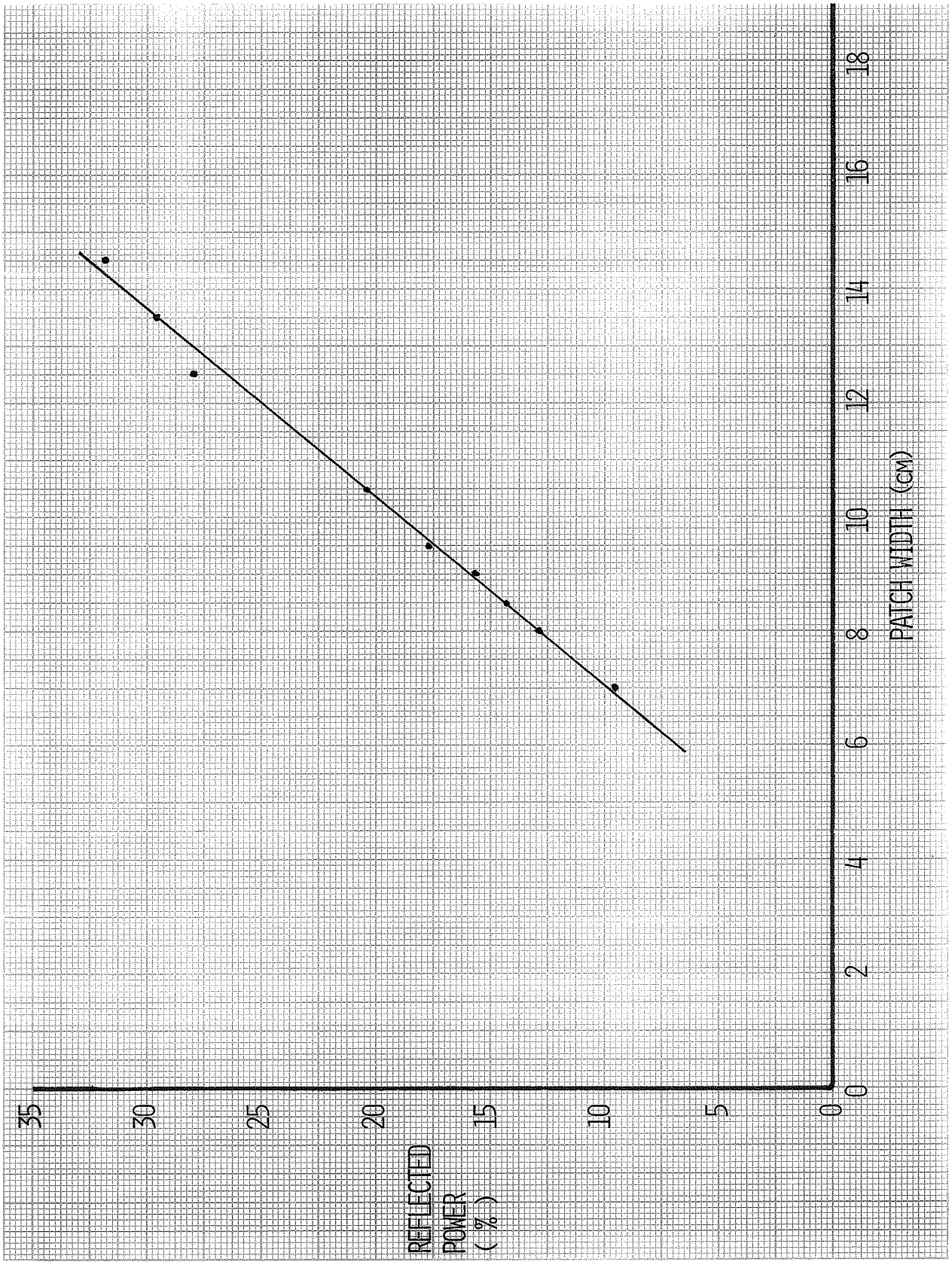

Figure 15. Reflected power percentage as a function of patch width for a MCT-85 microstrip antenna element.

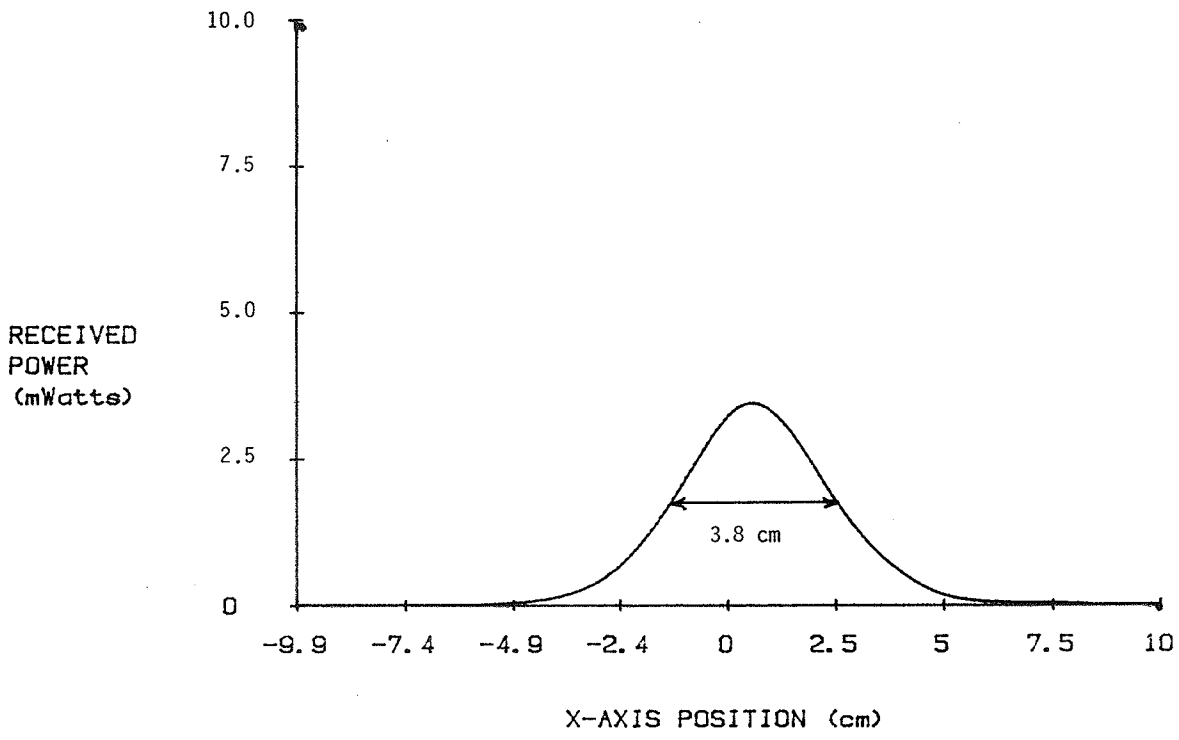

Figure 16. H-plane principal axis pattern plot of a single MCT-85 microstrip element.

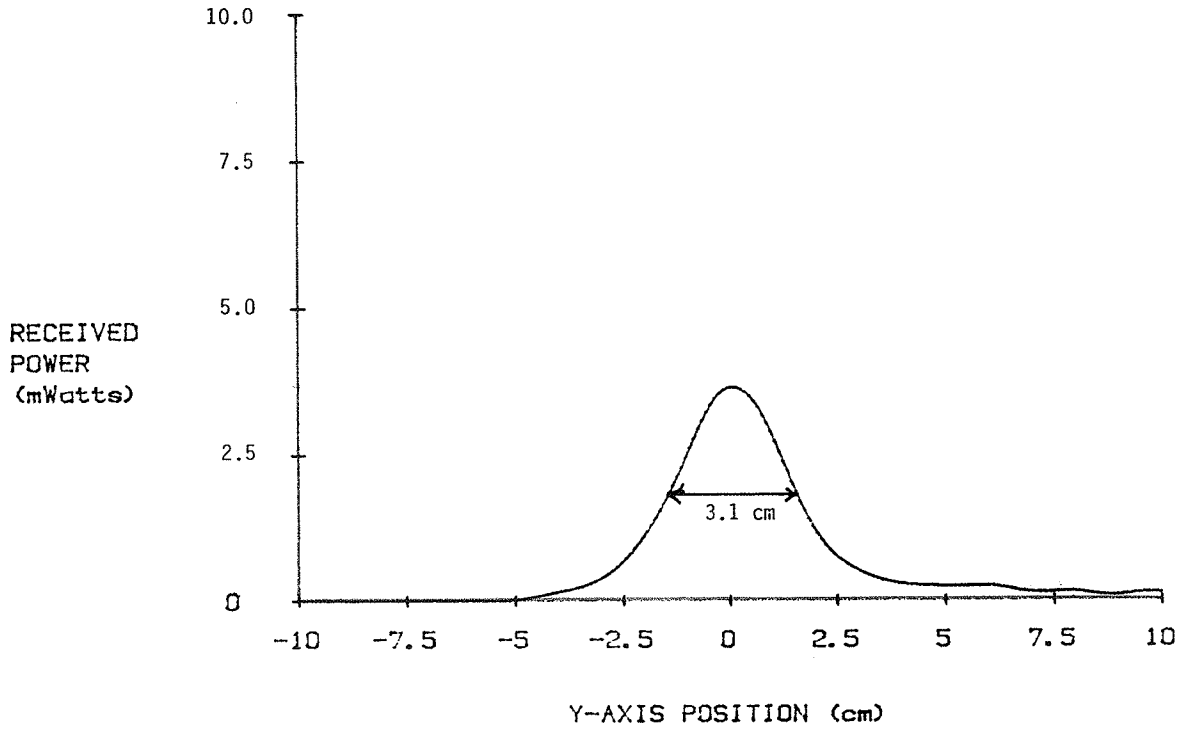

Figure 17. E-plane principal axis pattern plot of a single MCT-85 microstrip element.

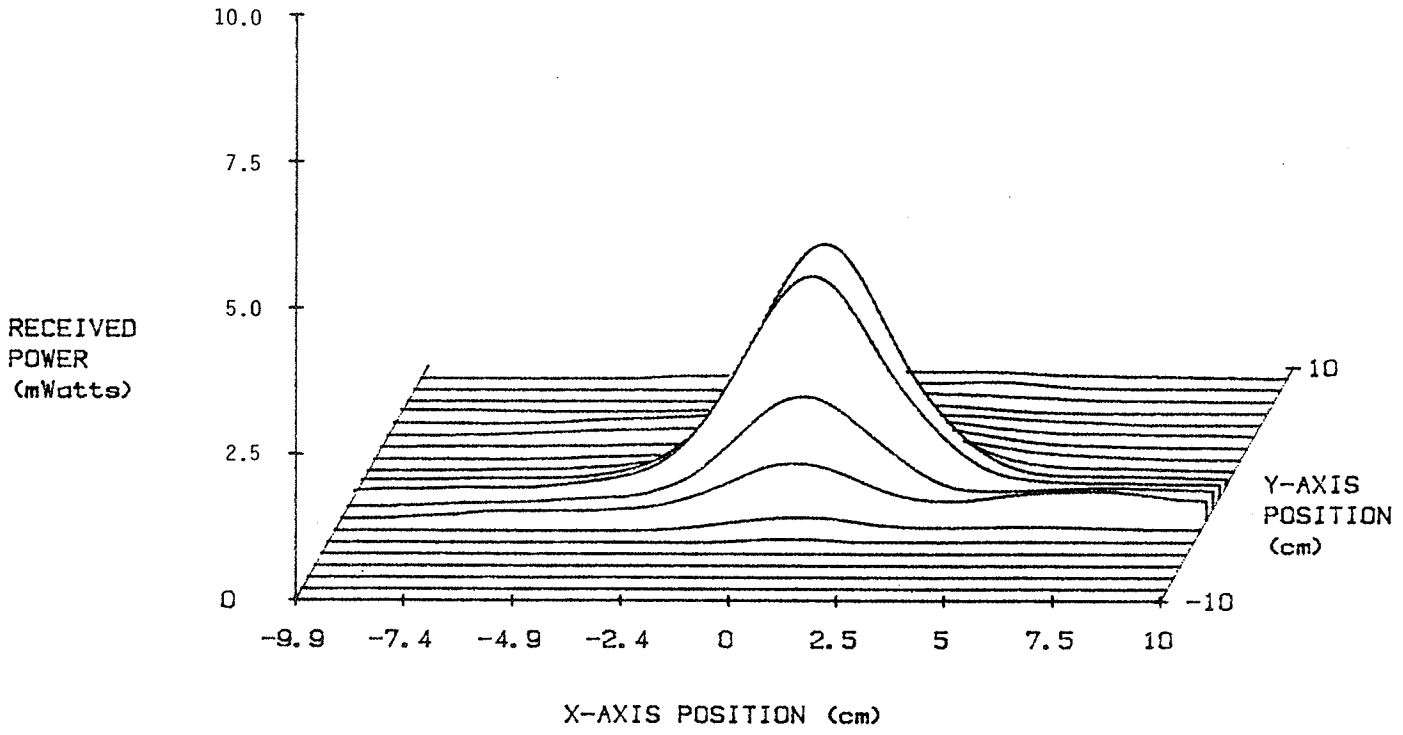

Figure 18. Contour pattern plot of a single MCT-85 microstrip element.

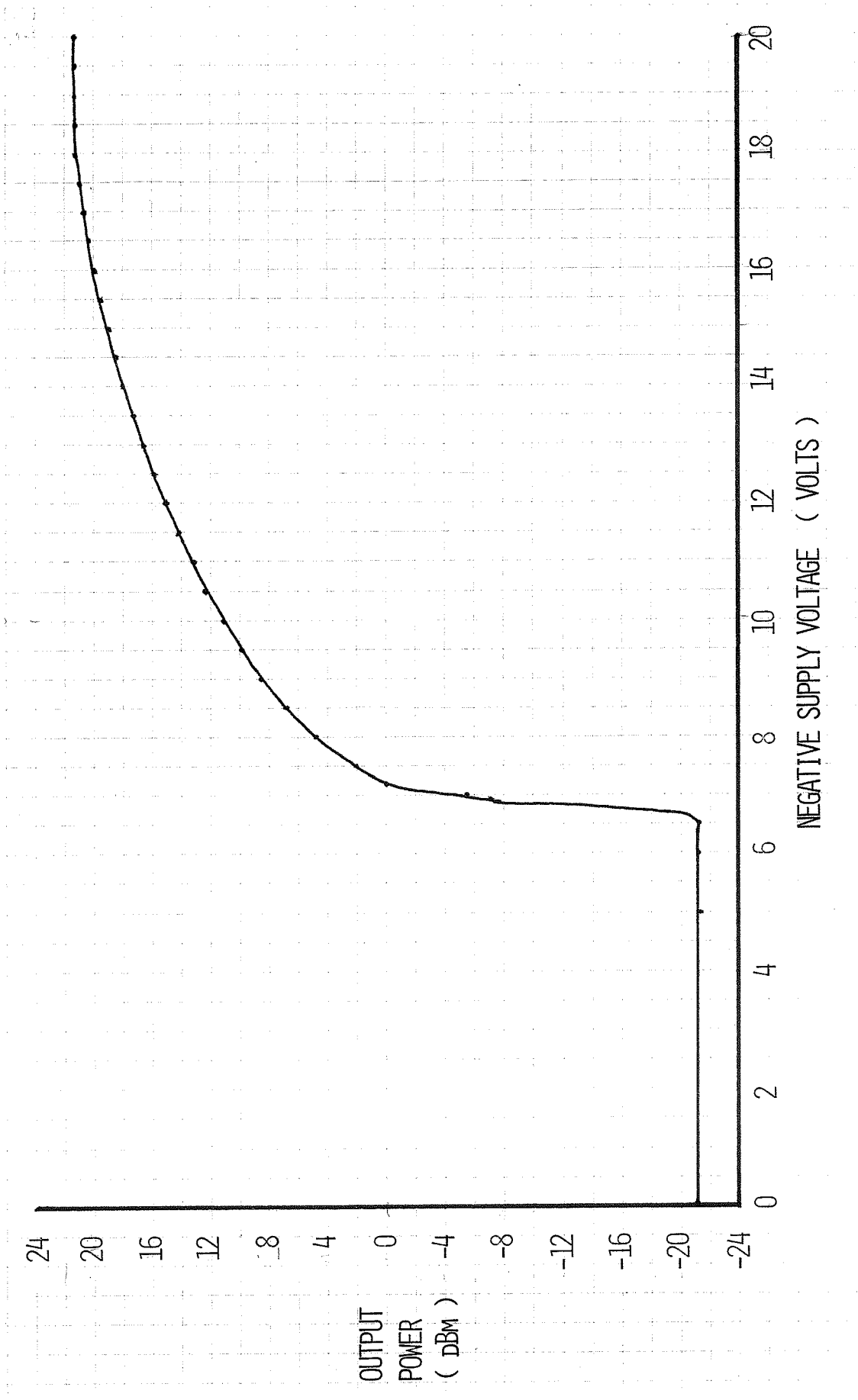

Figure 19. Output power vs. supply voltage for Engleman Microwave HFE 915 MHz source.

Absorptive Pin Diode Attenuator
Full octave electronic tuning with analog or digital input.

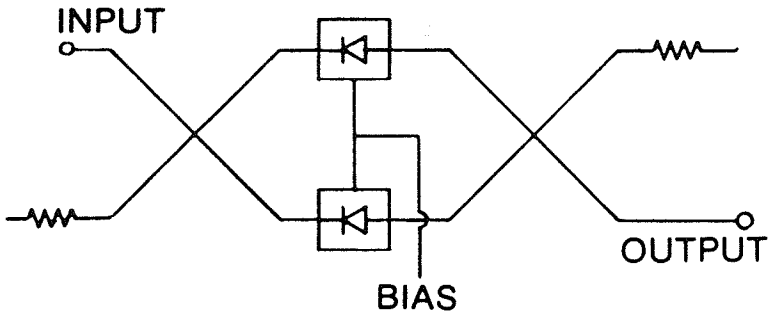

(a)

Digital Stepped Attenuator
Pin diode switched chip T-pads. For remote programming. Excellent flatness, VSWR, and temperature characteristics — high speed.

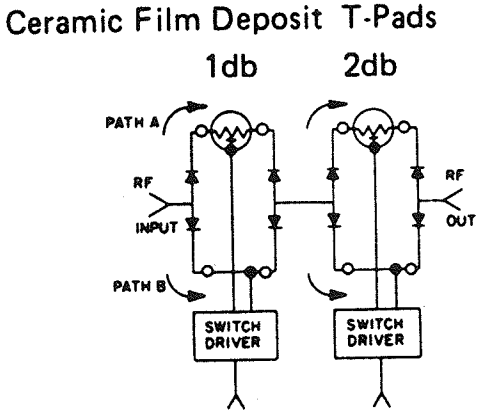

(b)

Figure 20. (a) Schematic of pin diode attenuator and (b) schematic of attenuator using cell structure [17].

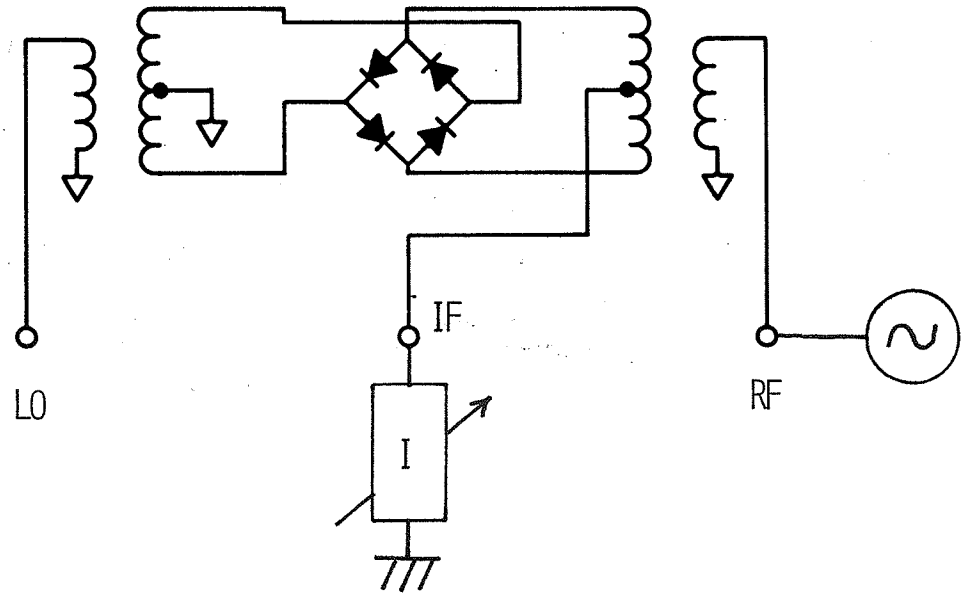

(a)

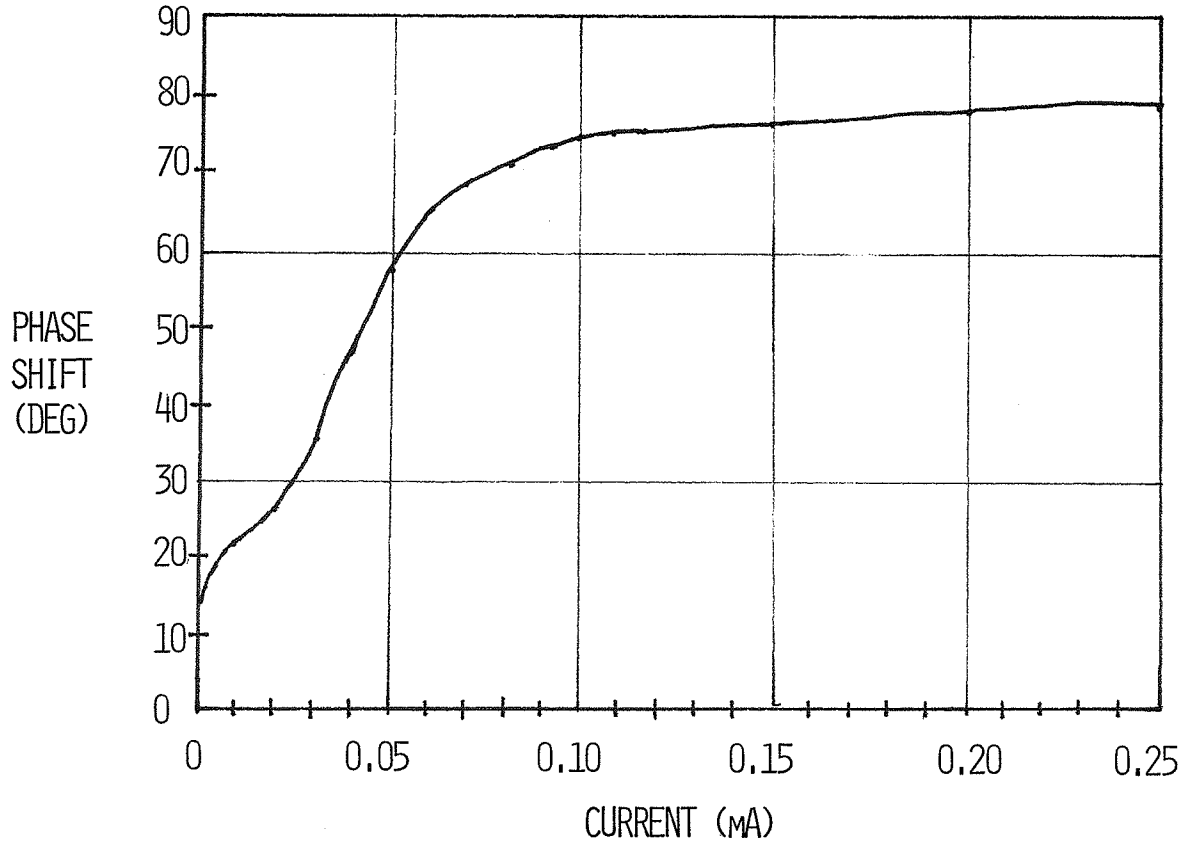

(b)

Figure 21. (a) Schematic of mixer used as phase shifter and (b) phase shift as a function of drive current for phase shifter in (a).

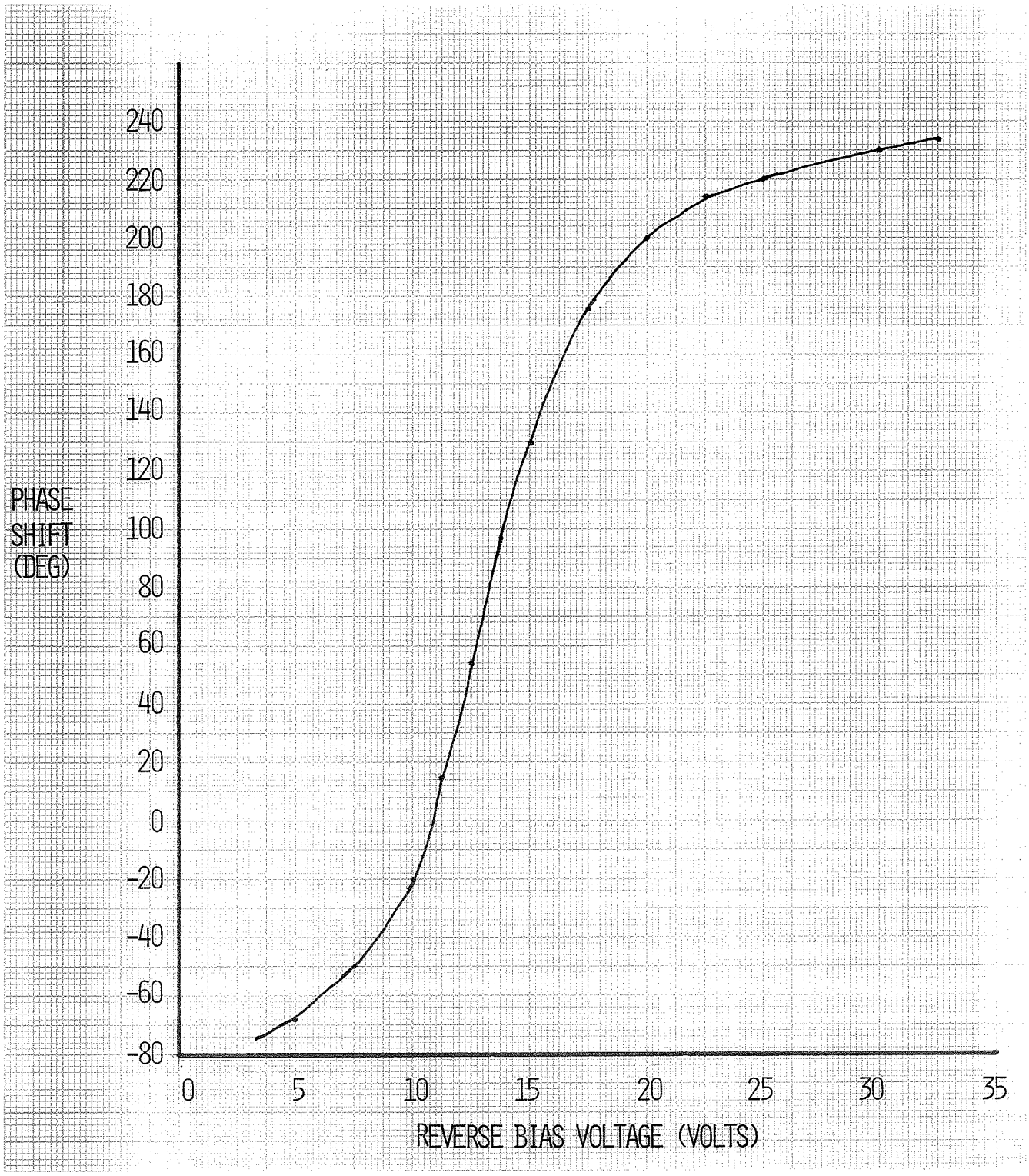

Figure 22. Phase shift as a function of reverse bias voltage for phase shifter constructed from 3 dB hybrid.

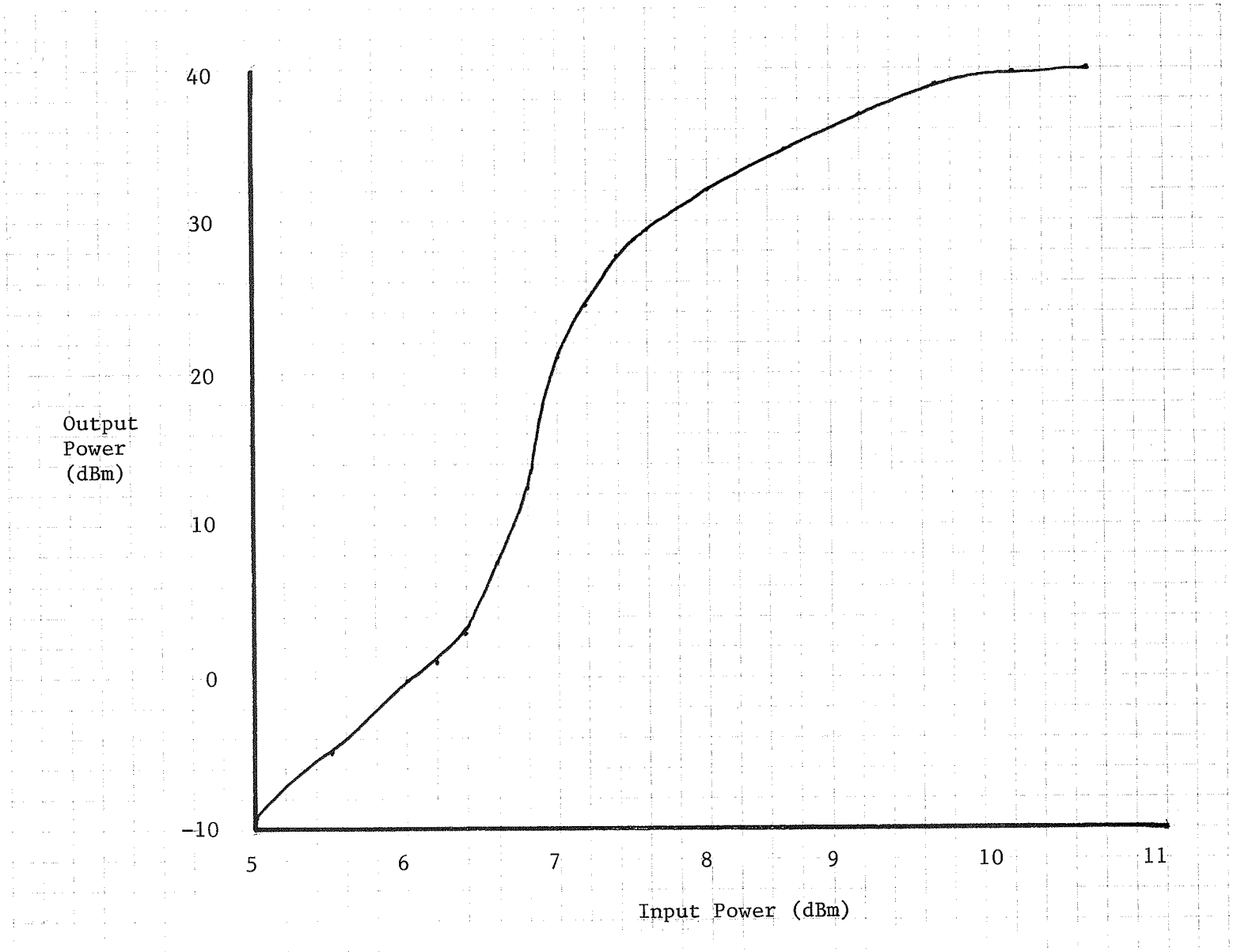

Figure 23. North Hills amplifier output power as a function of input power.

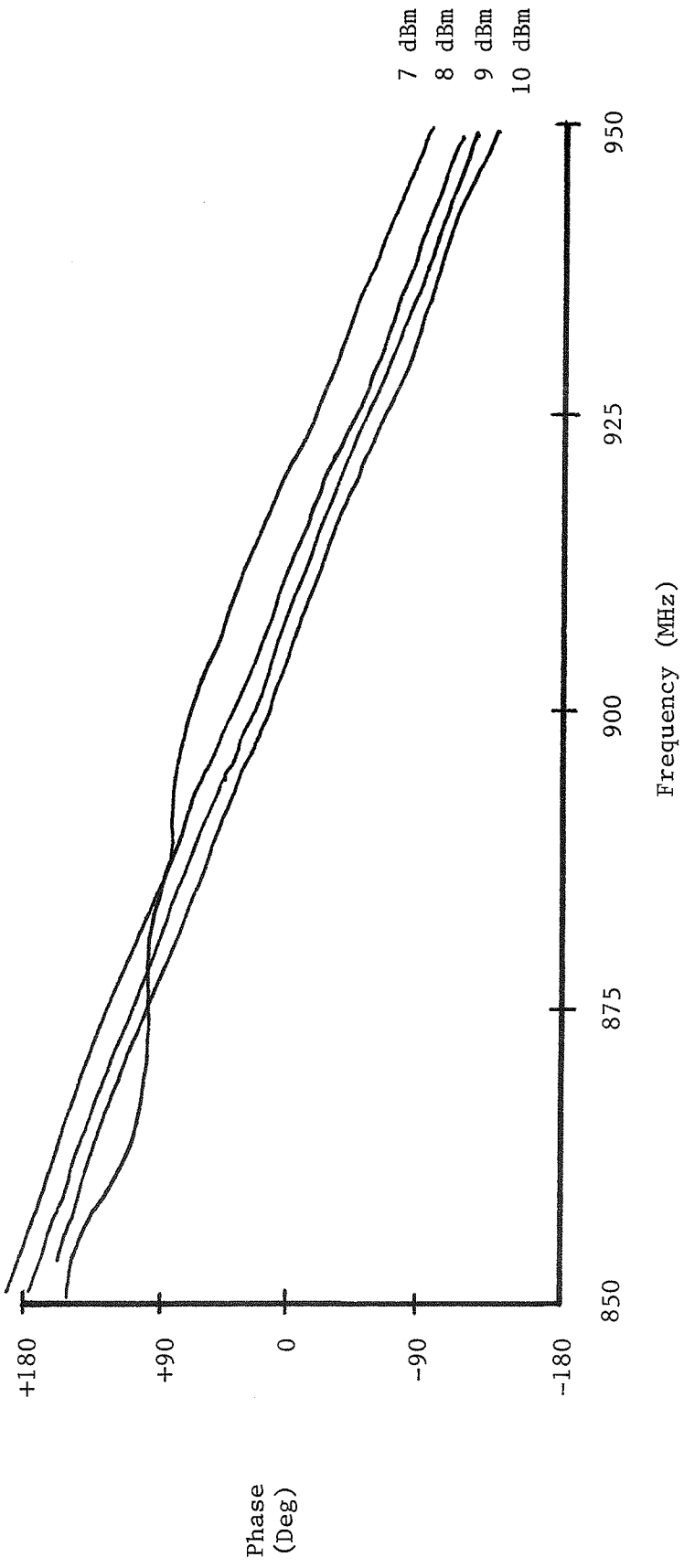

Figure 24. North Hills amplifier output signal phase as a function of frequency for varying input powers.

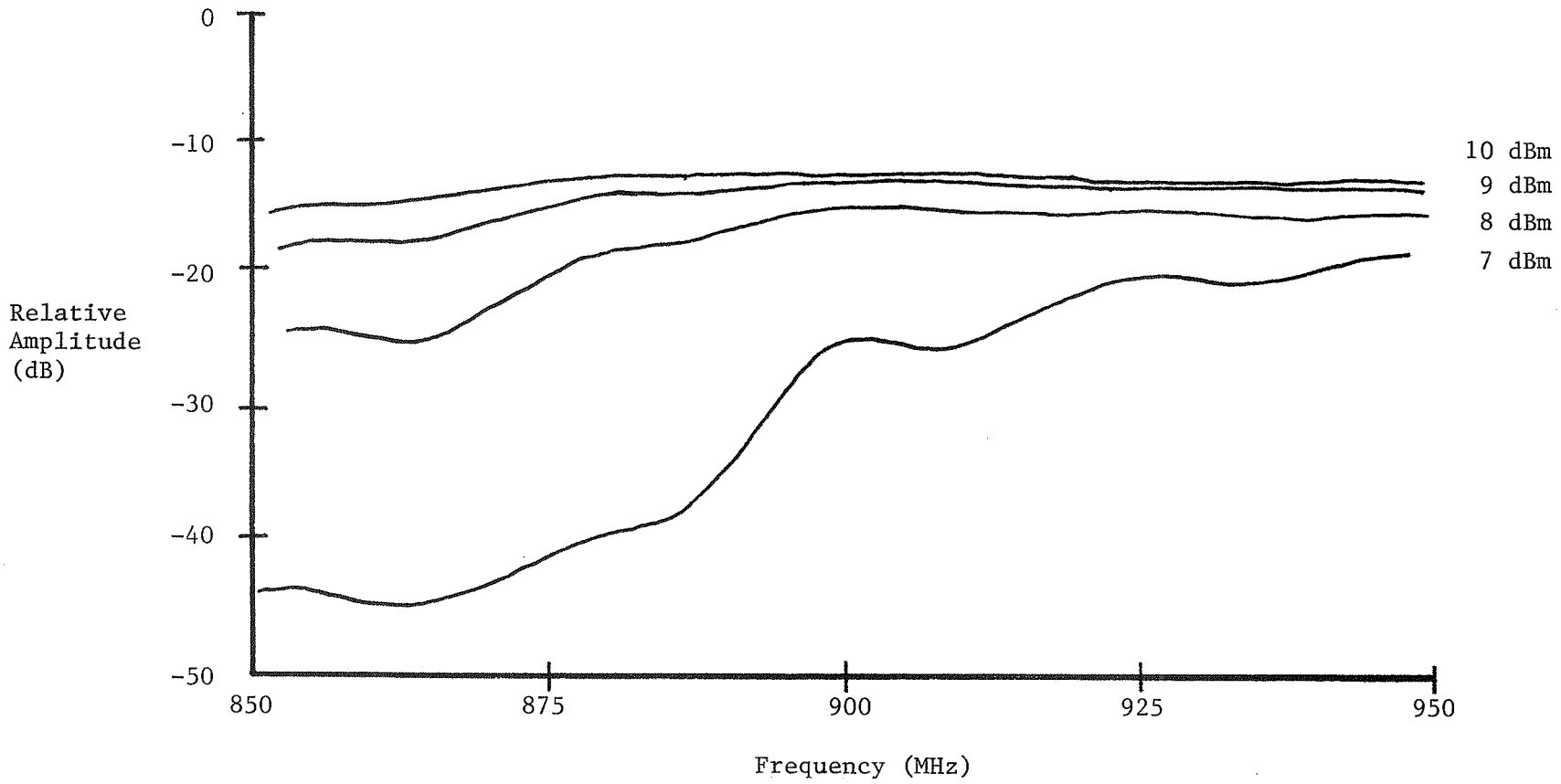

Figure 25. North Hills amplifier output signal amplitude as a function of frequency for varying input powers.

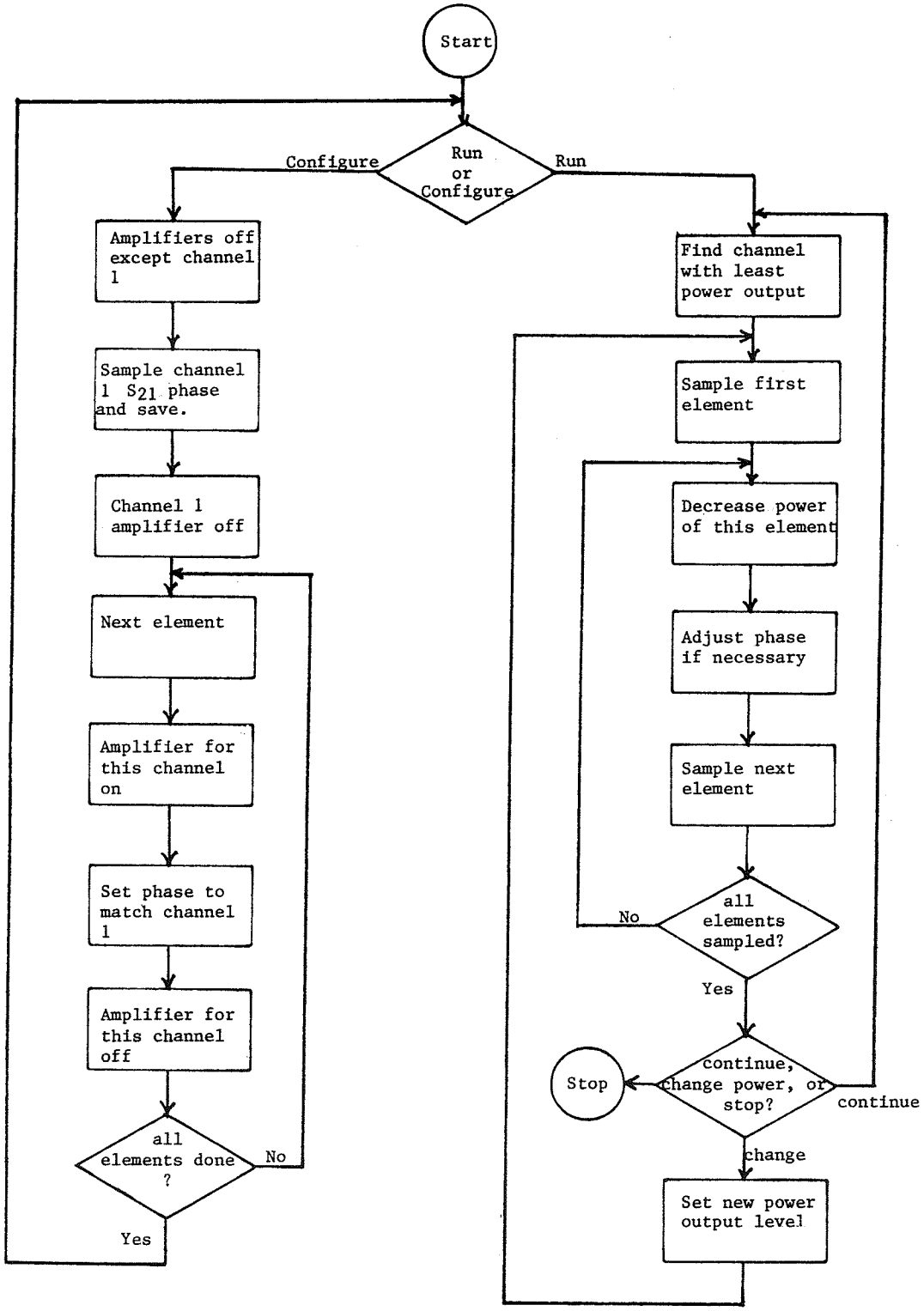

Figure 26. Control software flowchart for phased array hyperthermia system.

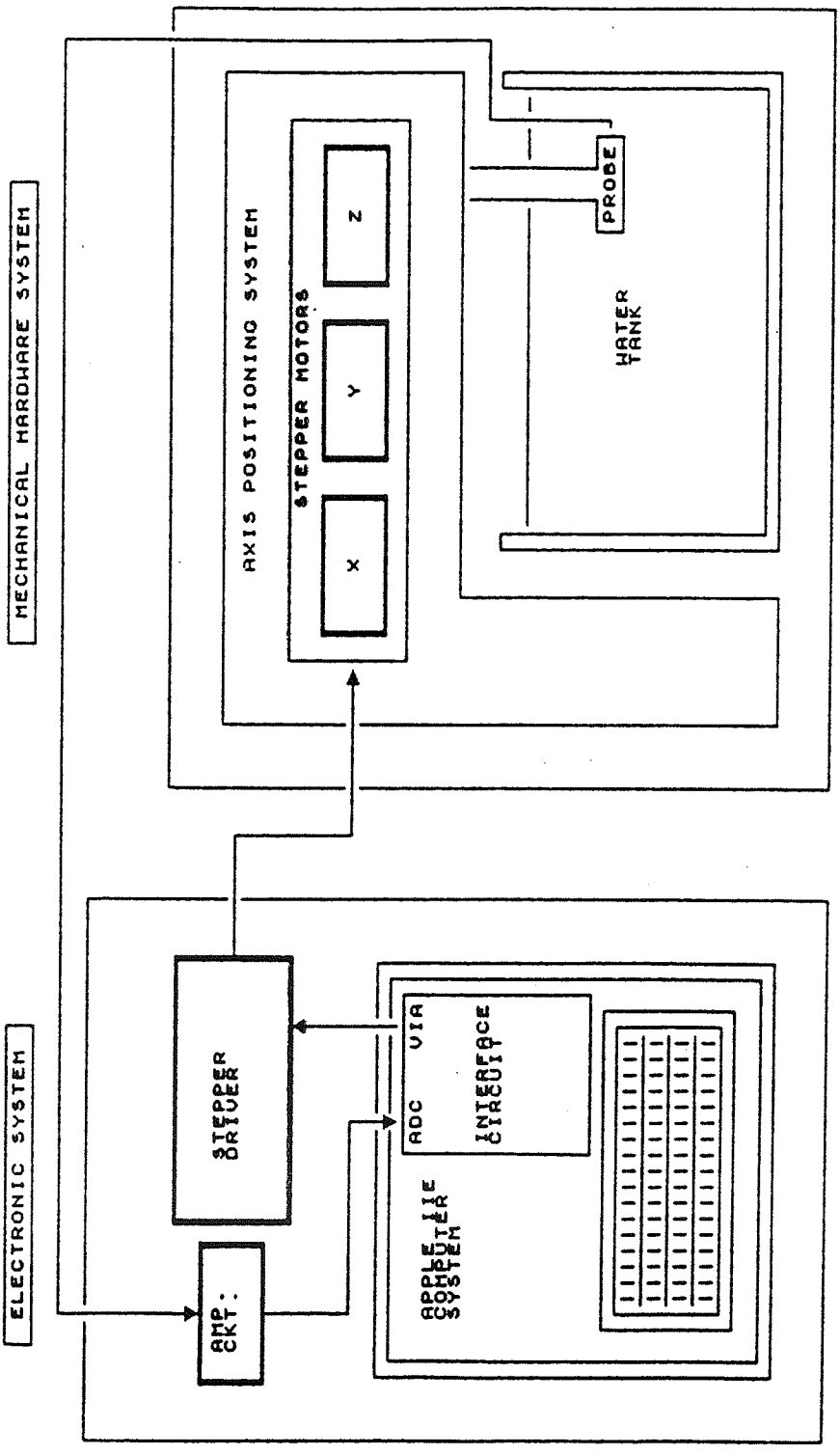

Figure 27. Three-axis computer controlled scanner and data aquisition system block diagram [14].

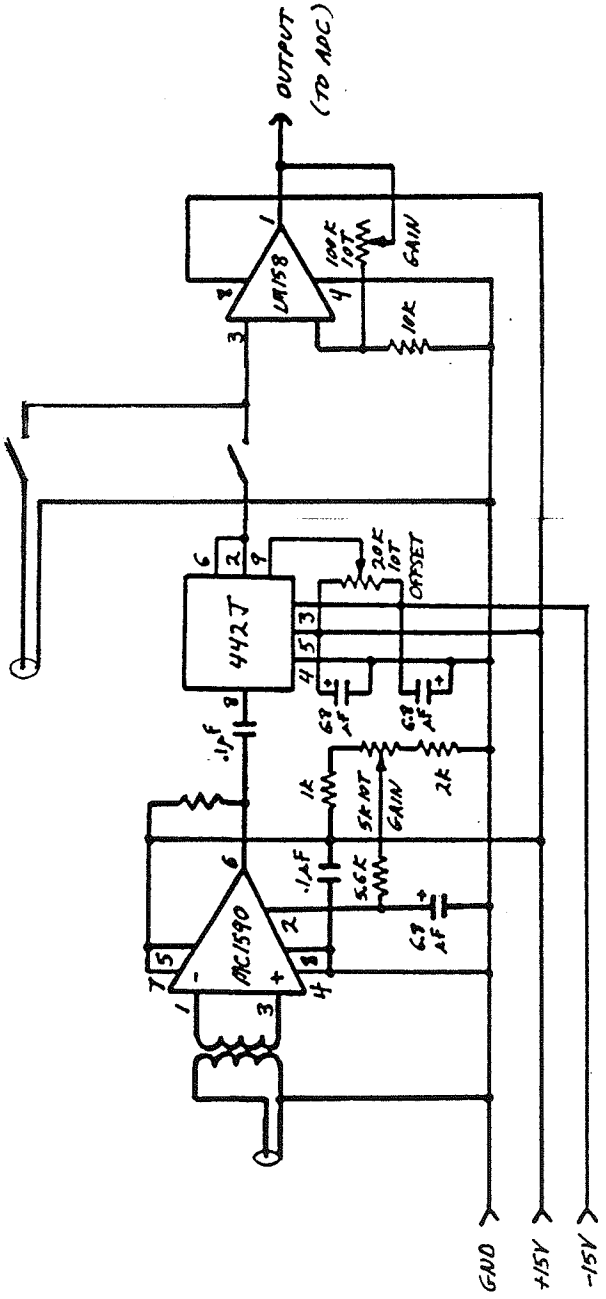

Figure 28. Modified amplifier circuitry.

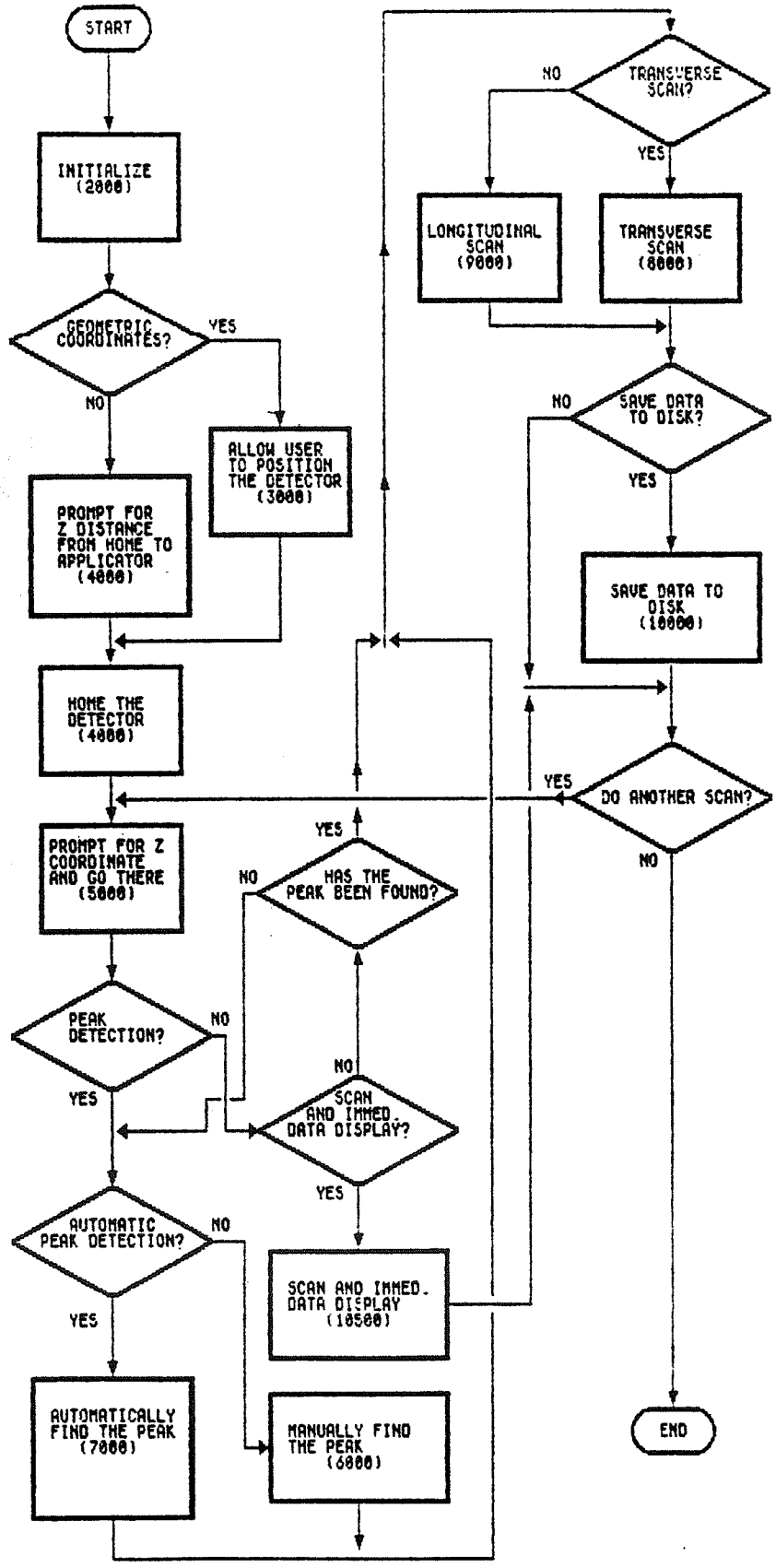

Figure 29. Original scanner control software flowchart [14]

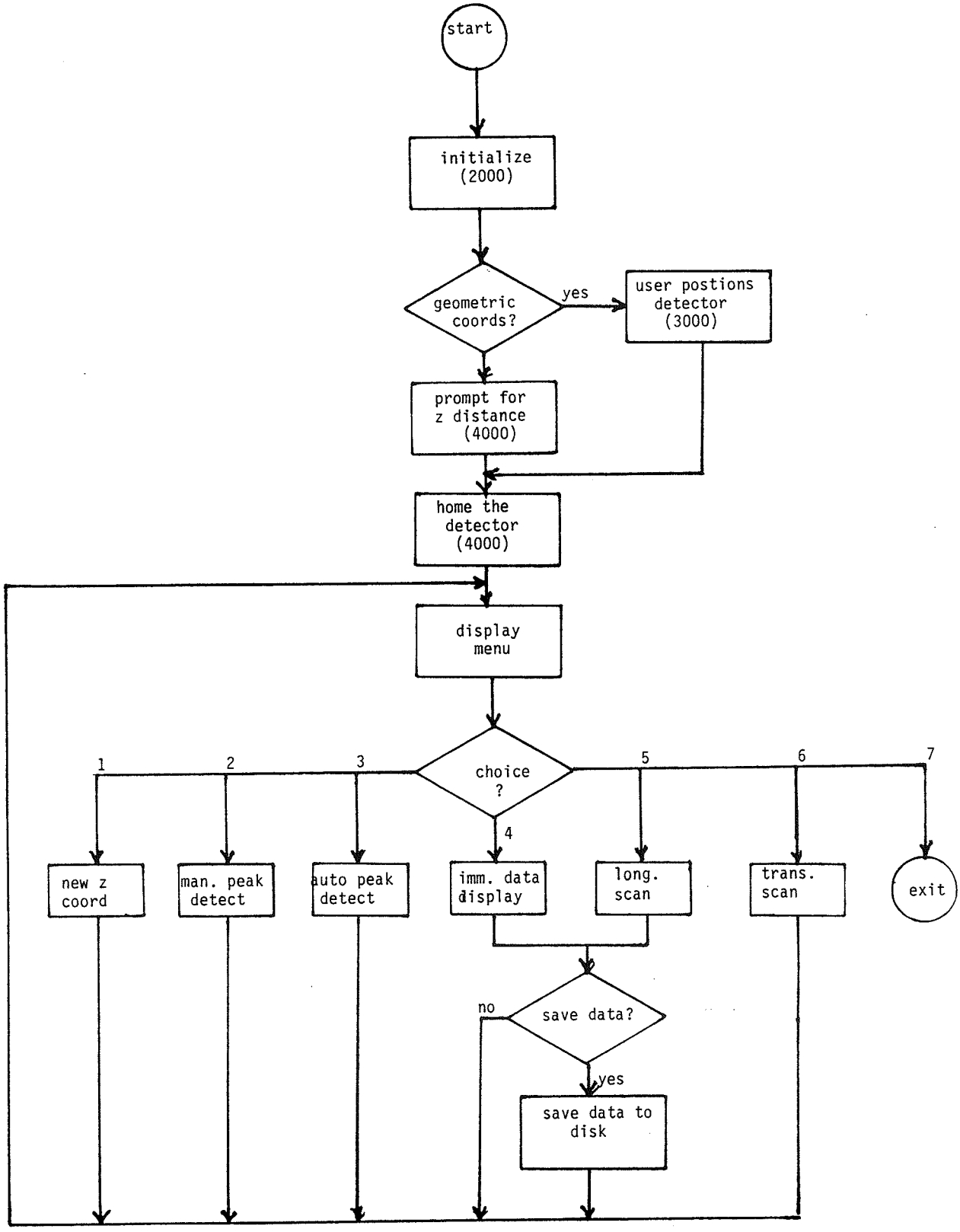

Figure 30. Revised scanner control software flowchart.

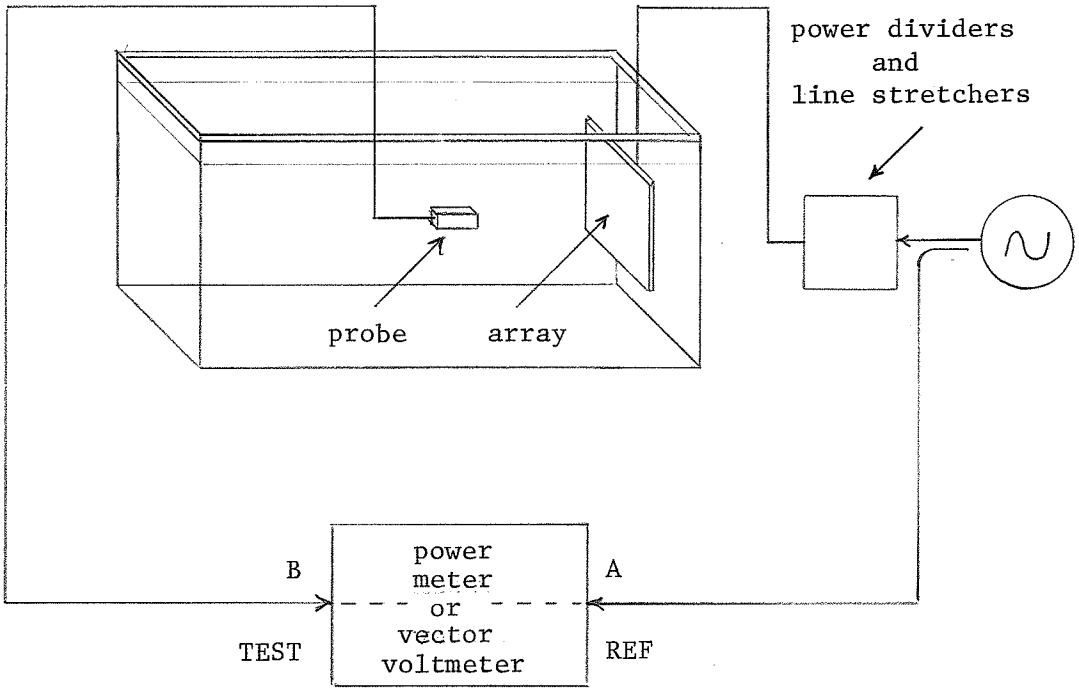

(a)

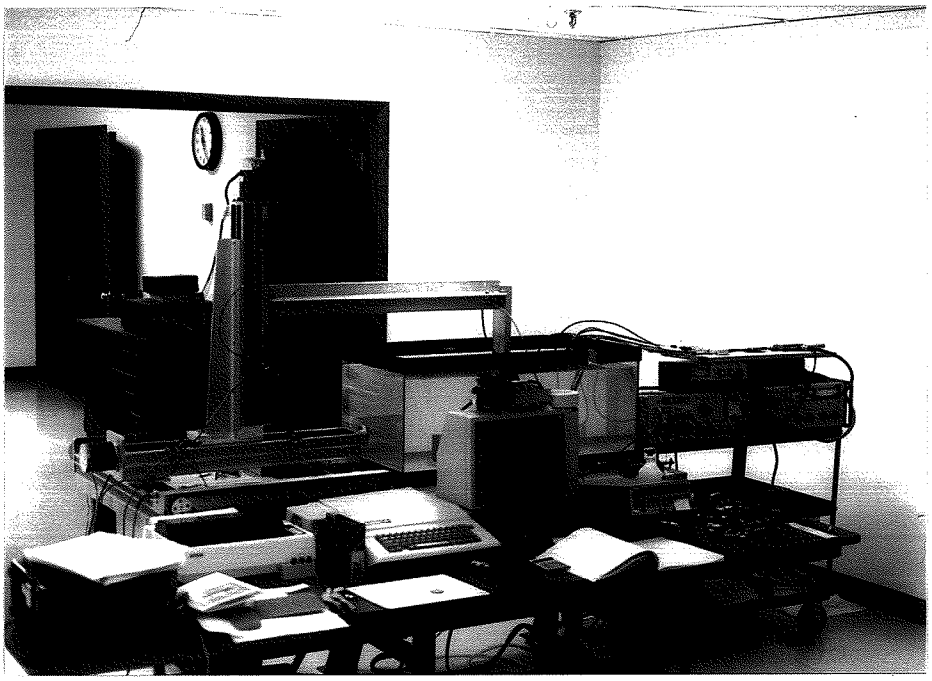

(b)

Figure 31. (a) Test bench diagram and (b) photo.

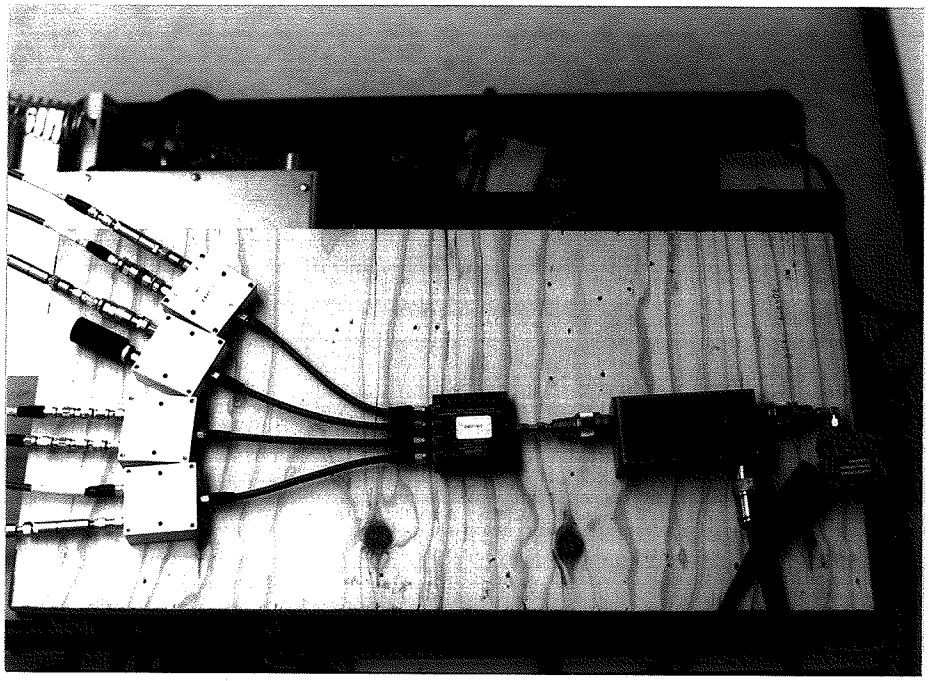

Figure 32. Photo of power distribution network showing (right to left) source, directional coupler, power dividers, and line stretchers.

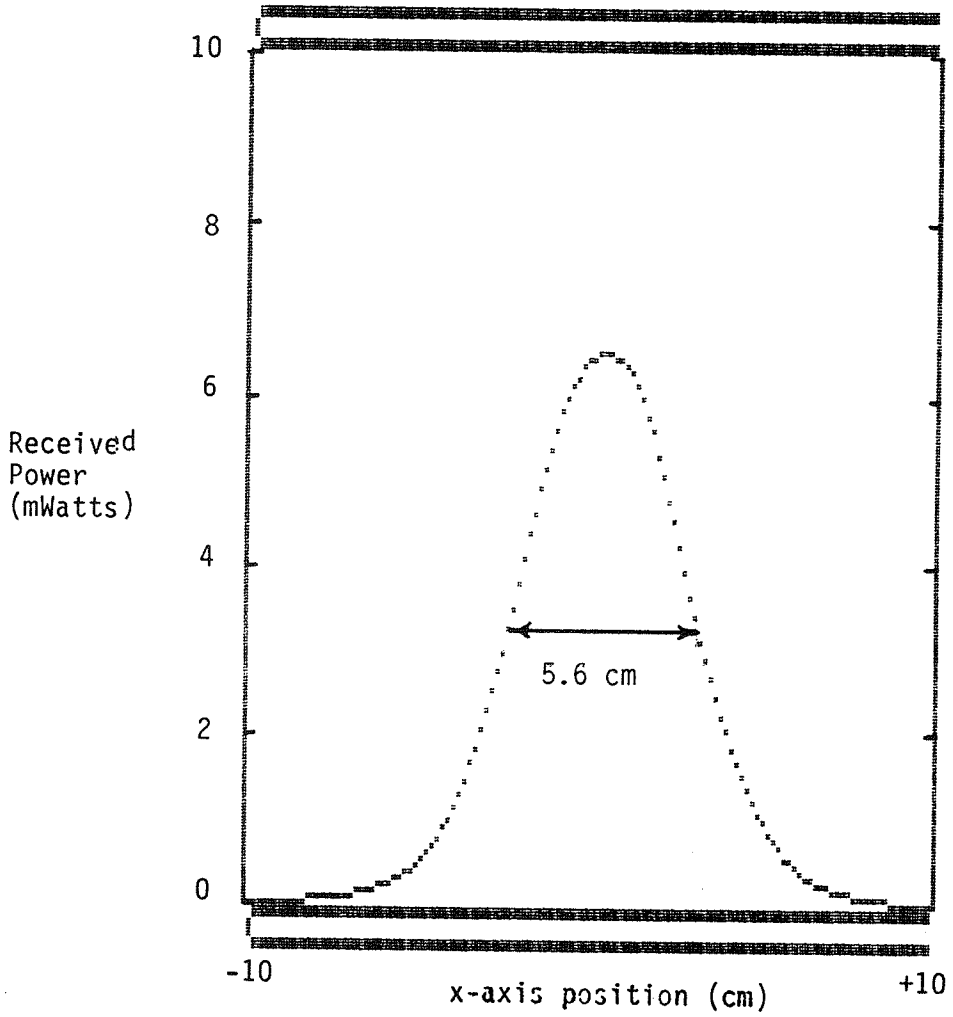

Figure 33. H-Plane principal axis pattern plot of seven element PC board microstrip phased array focused at (0,0,4).

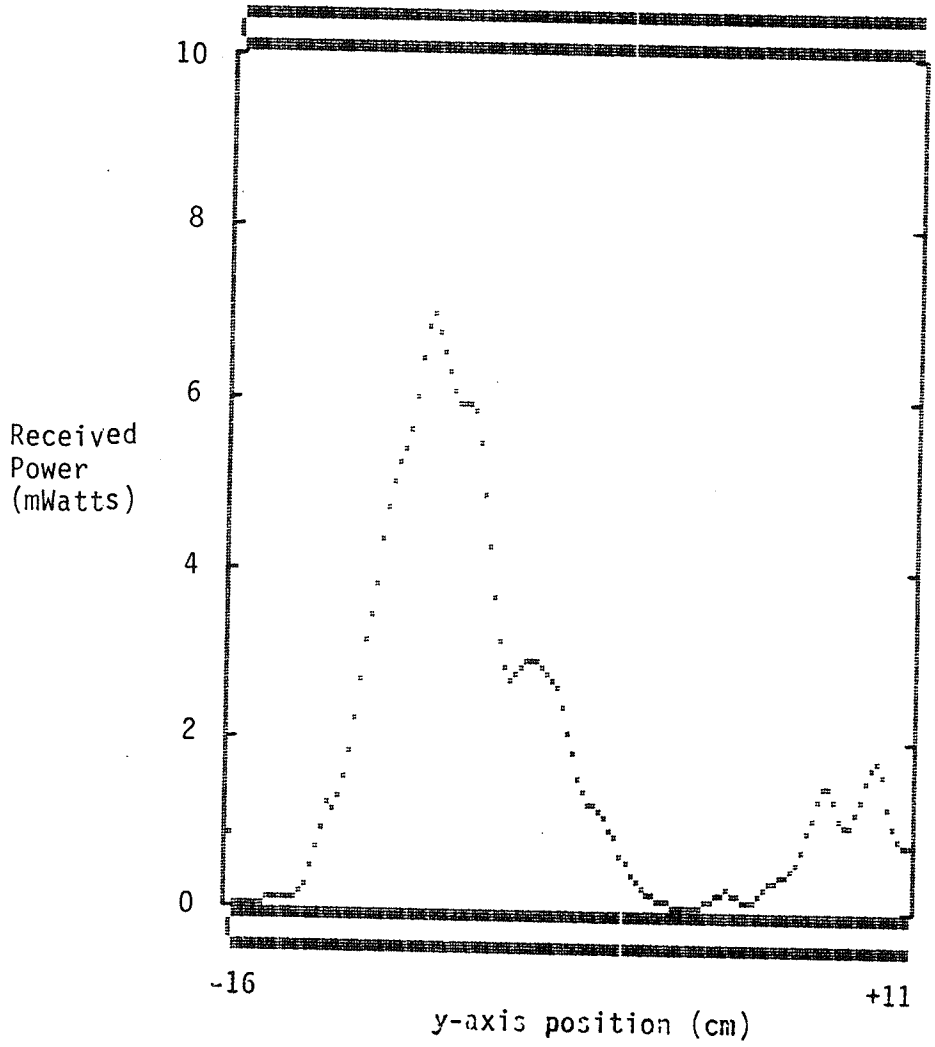

Figure 34. E-plane principal axis pattern plot of seven element PC board microstrip phased array focused at (0,0,4).

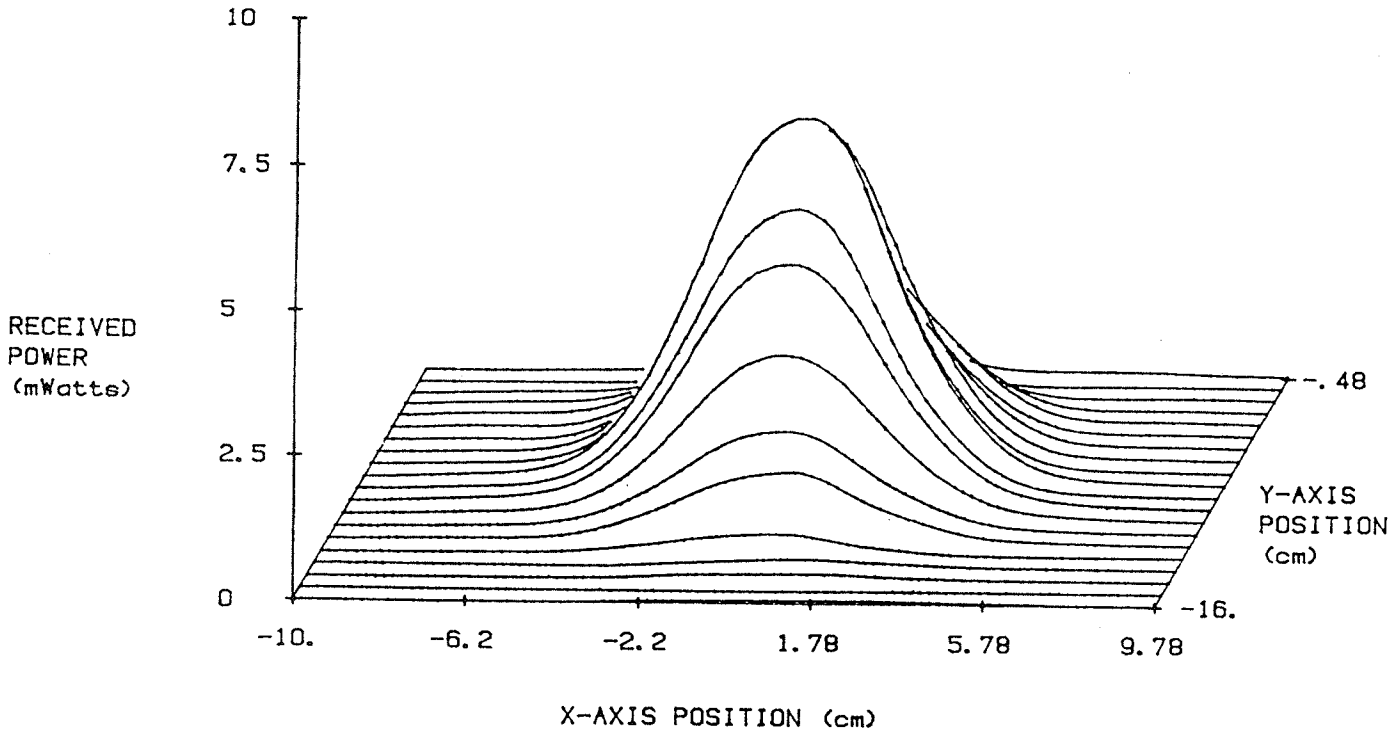

Figure 35. Contour pattern plot of seven element PC board microscrip phased array focused at (0,0,4).

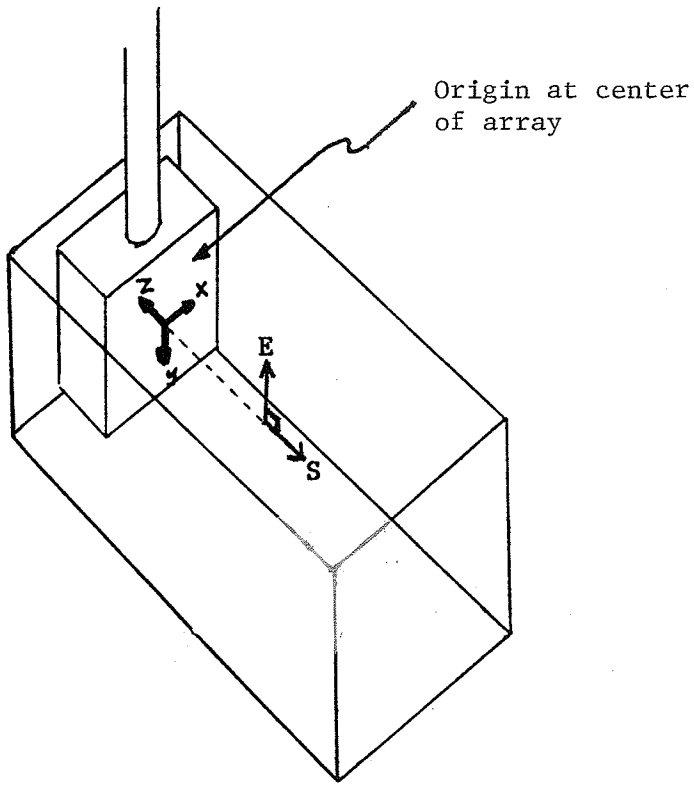

Figure 36. Coordinate system for scanner measurements.

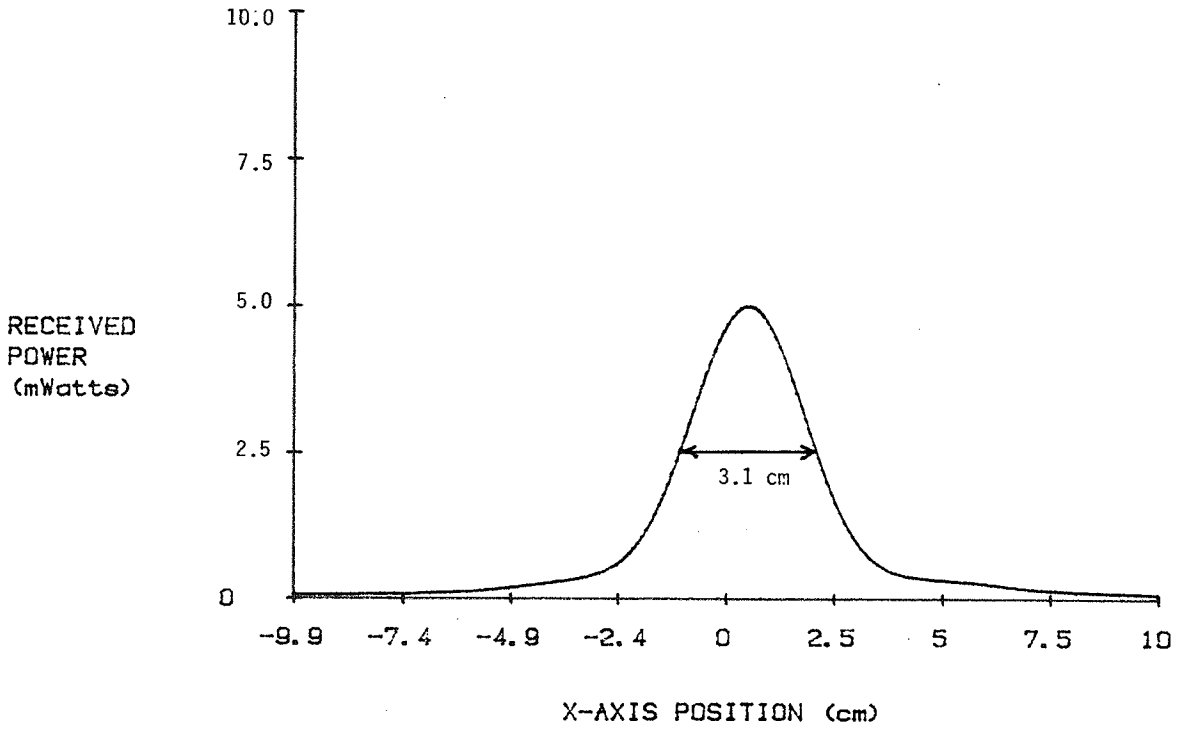

Figure 37. H-Plane principal axis pattern plot of seven element MCT-85 phased array focused at (0,0,4).

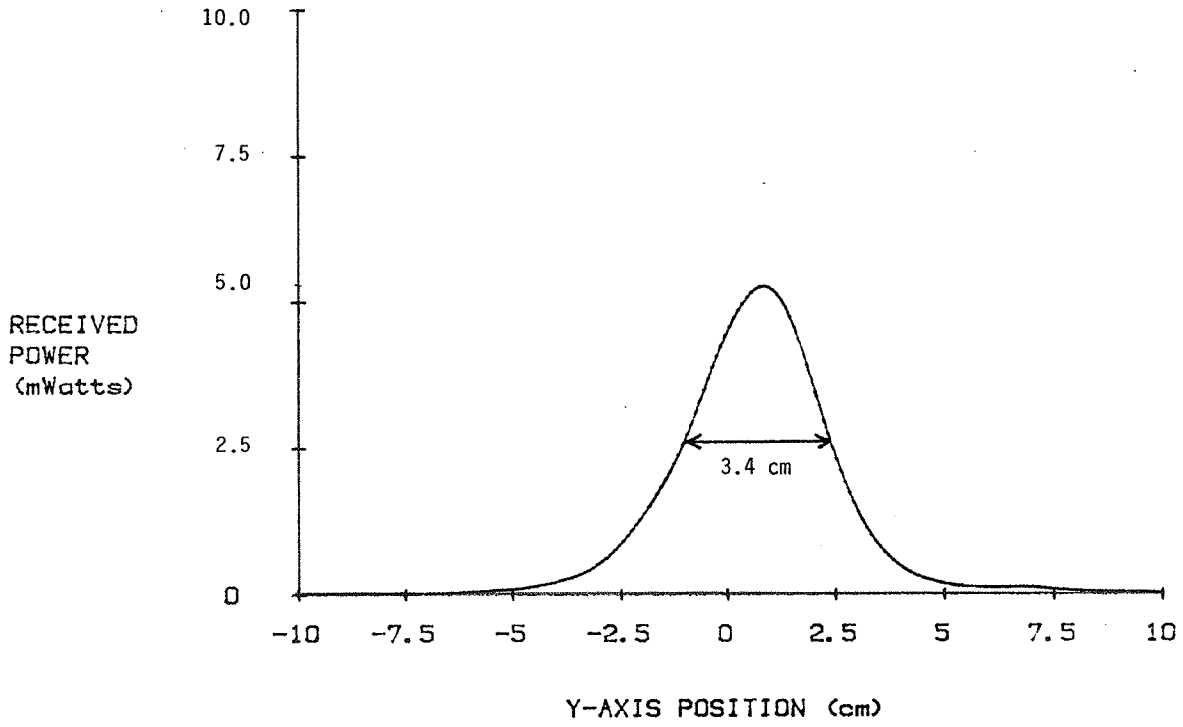

Figure 38. E-plane principal axis pattern plot of seven element MCT-85 phased array focused at (0,0,4).

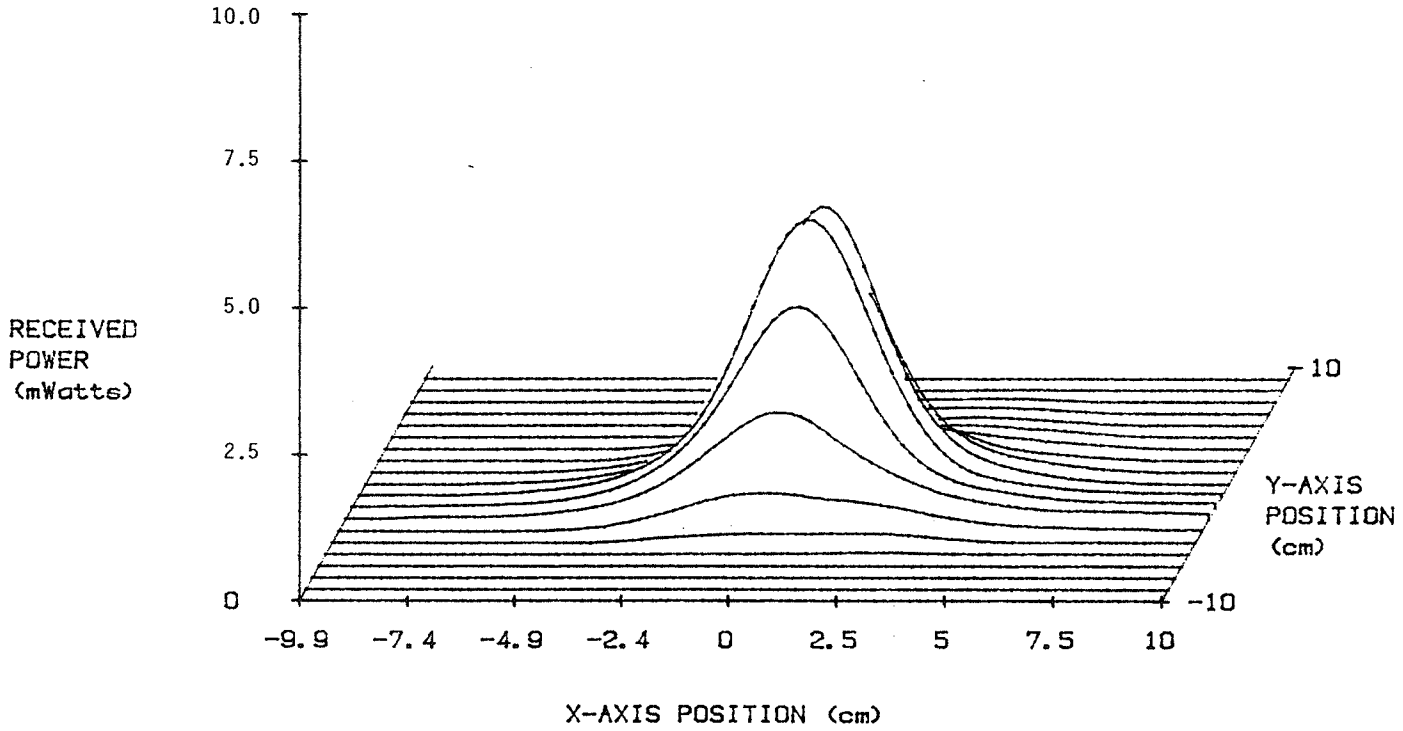

Figure 39. Contour pattern plot of seven element MCT-85 phased array focused at (0,0,4).

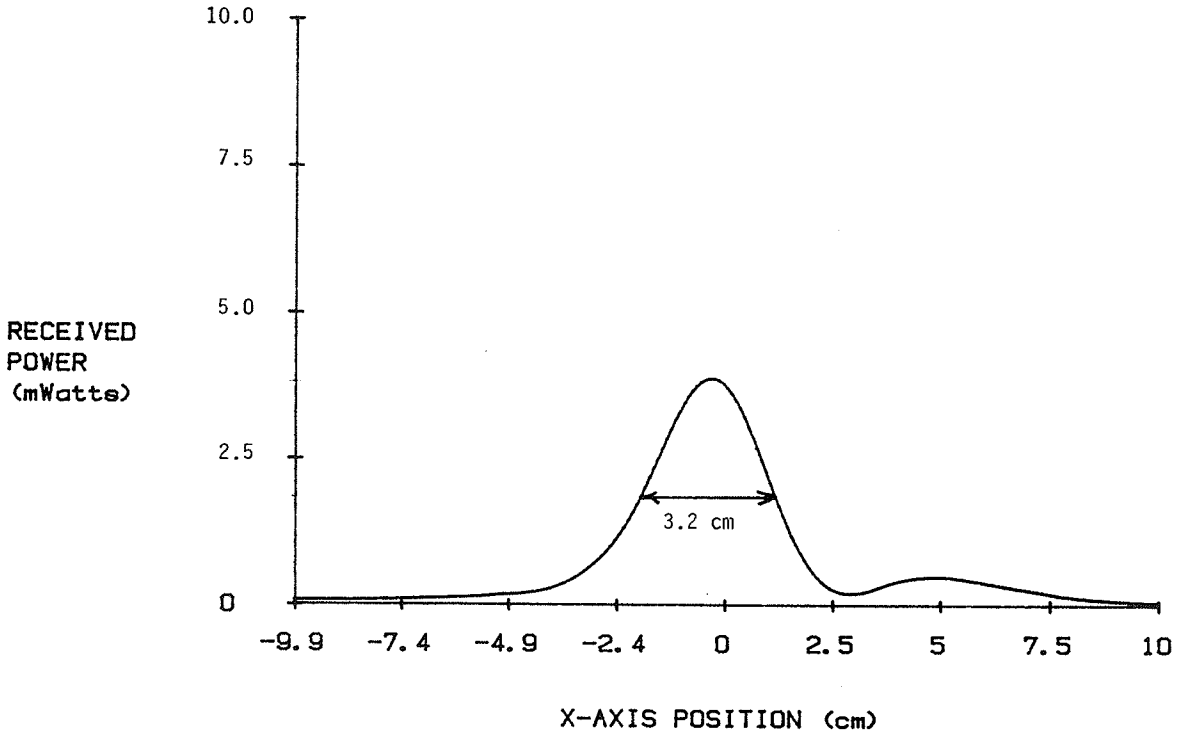

Figure 40. H-plane principal axis pattern plot of seven element MCT-85 phased array focused at (-1.5,3,4).

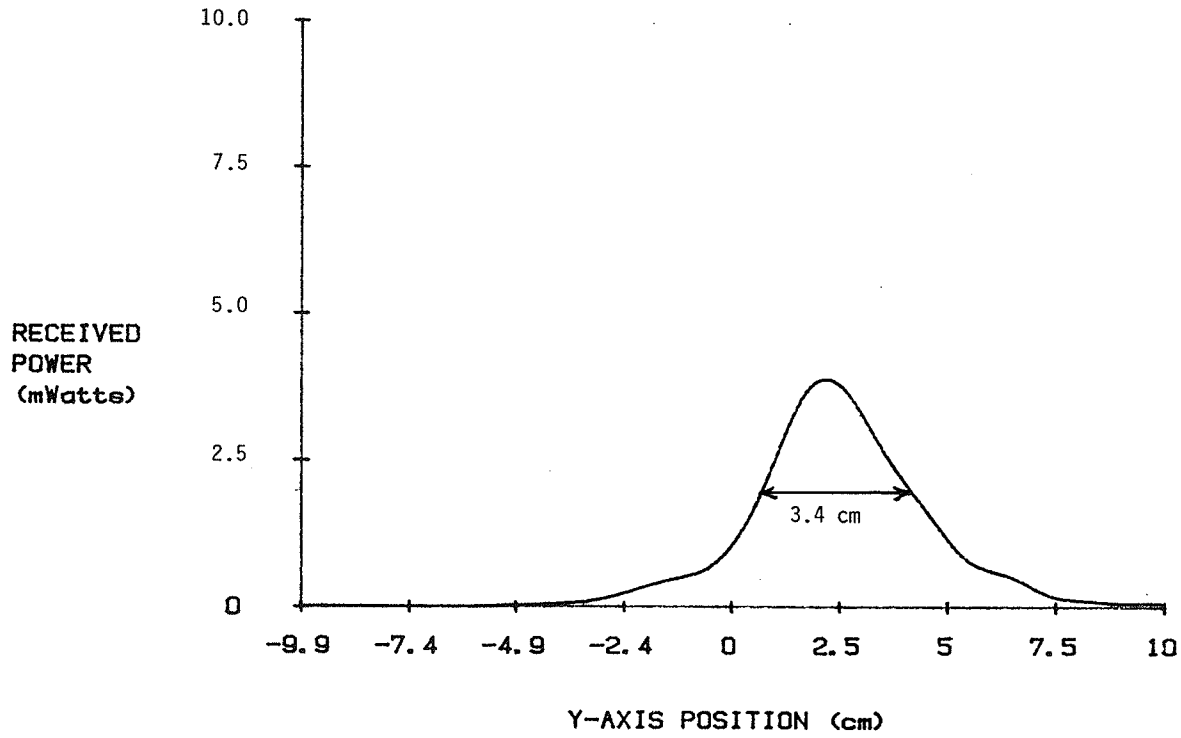

Figure 41. E-plane principal axis pattern plot of seven element MCT-85 phased array focused at (-1.5,3,4).

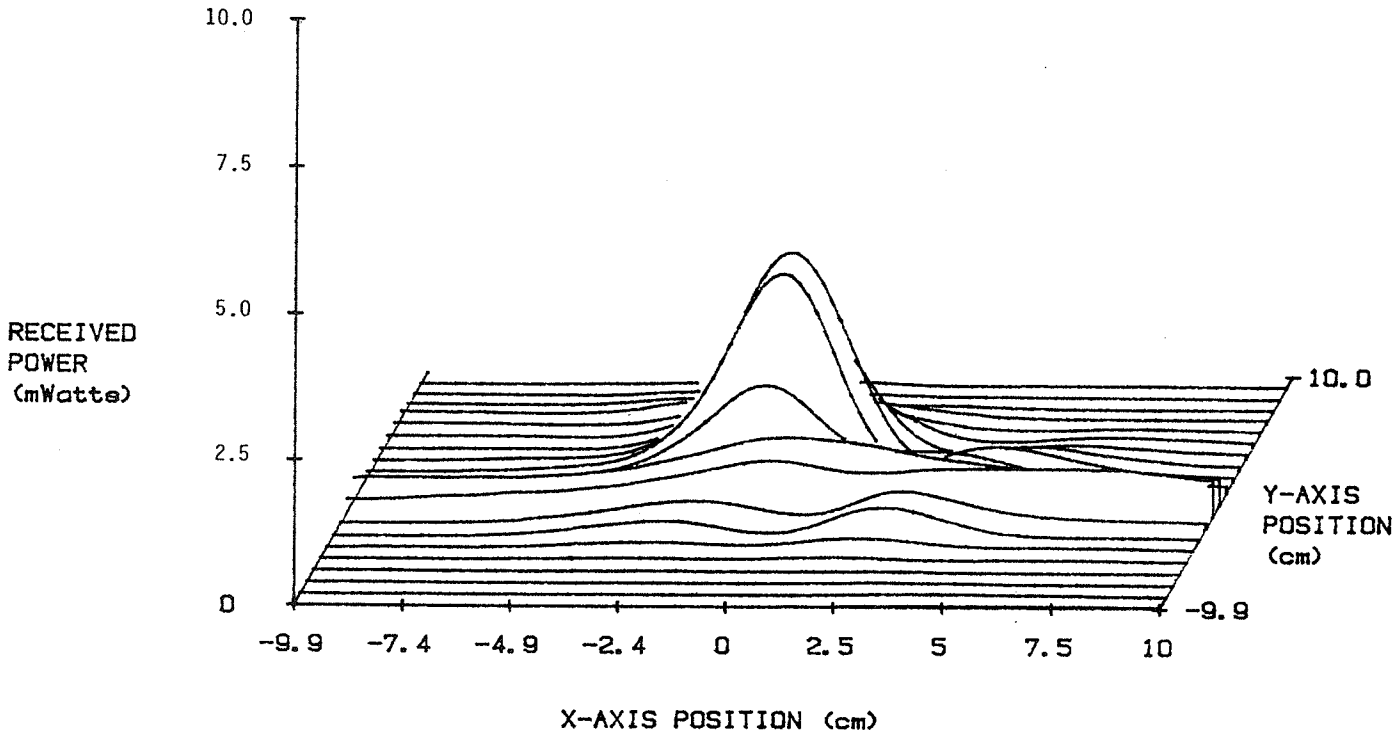

Figure 42. Contour pattern plot of seven element MCT-85 phased array focused at (-1.5,3,4).

APPENDIX - LISTING OF TRANSVERSE.PLOT

```
5  REM  ============================================================
10  REM
15  REM   Program:  TRANSVERSE.PLOT
20  REM   Revision Date:  5/2/85
25  REM  Programmer: Tim Benson
30  REM
110  REM    This program reads the descriptor file of a set of scanner
120  REM   data files, displays the data format, and then asks if the
130  REM   user wishes to plot the data.  If the data is to be plotted,
140  REM   the plotter is initialized, and then the data is plotted,
150  REM   the data having been stored on disk in 8K chunks in files
160  REM   with sequential filenames, e.g. filename.0, filename.1,
170  REM   filename.2, etc.
180  REM   ============================================================
190 D$ =  CHR$ (4)
200 BL$ =  CHR$ (7)
210 ET$ =  CHR$ (3)
220 CM = 0.00127
225 T1 = 0
230  PRINT D$;"PR#3"
240  DIM A(9)
245  DIM G(3)
250  DIM B$(9)
260  DIM ZMAX(300)
270  FOR I = 1 TO 300:ZMAX(I) =  - 9999: NEXT I
280  HOME
290  INPUT "ENTER FILE NAME:  ";F$
300  PRINT D$;"OPEN ";F$
310  PRINT D$;"READ ";F$
320  INPUT GC$: INPUT DL: INPUT TS$
330  INPUT G(1): INPUT G(2): INPUT G(3)
430  FOR N = 1 TO 3
440  INPUT A(N)
450 A(N) = (A(N) - G(N)) * CM
460 B$(N) =  LEFT$ ( STR$ (A(N)),6)
470  NEXT N
471  FOR N = 4 TO 9
472  INPUT A(N)
473 A(N) = A(N) * CM
474 B$(N) =  LEFT$ ( STR$ (A(N)),6)
475  NEXT N
480  PRINT D$;"CLOSE ";F$
490  HOME
500  PRINT "FILE NAME          ";F$
510  IF GC$ = "Y" THEN  PRINT "COORDINATE SYSTEM: GEOMETRIC"
520  IF GC$ <  > "Y" THEN  PRINT "COORDINATE SYSTEM: TANK"
530  IF TS$ = "Y" THEN  PRINT "SCAN TYPE:         TRANSVERSE"
540  IF TS$ <  > "Y" THEN  PRINT "SCAN TYPE:         LONGITUDINAL"
550  PRINT
560  PRINT
570  PRINT "X-AXIS";: HTAB 15: PRINT "Y-AXIS";: HTAB 30: PRINT "Z-AXIS"
580  PRINT "------";: HTAB 15: PRINT "------";: HTAB 30: PRINT "------"
590  PRINT B$(1);: HTAB 15: PRINT B$(2);: HTAB 30: PRINT B$(3);: HTAB 40:
```

```
     PRINT "======> CENTER COORDINATES (CM)"
600  PRINT B$(4);: HTAB 15: PRINT B$(5);: HTAB 30: PRINT B$(6);: HTAB 40:
     PRINT "======> SCAN RANGES (CM)"
610  PRINT B$(7);: HTAB 15: PRINT B$(8);: HTAB 30: PRINT B$(9);: HTAB 40:
     PRINT "======> SCAN INCREMENTS (CM)"
620  IF TS$ <  > "Y" THEN  GOTO 810
625  REM
630  REM  Compute # of data points along x-axis.  If both the x scan
640  REM  range and x scan increment are zero, only one point was taken
650  REM   on this axis.  Otherwise, the number of points is twice the
660  REM  x scan range divided by the scan increment, plus one.
665  REM
670  IF A(4) + A(7) = 0 THEN XX = 1: GOTO 700
680 XX = (2 * A(4)) / A(7) + 1
690  REM  Compute # of data points along y-axis.  (See note for x-axis)
700  IF A(5) + A(8) = 0 THEN YY = 1: GOTO 750
710 YY = (2 * A(5)) / A(8) + 1
715  REM
720  REM  The total number of data points taken is the product of the
730  REM  number of points along the x-axis, and the number of scans
740  REM  (the number of y-axis scans)
745  REM
750 NM =  INT (XX * YY + 0.1)
760  GOTO 820
765  REM
770  REM  If this was a longitudinal scan, the number of data points
780  REM  taken is twice the z-axis range divided by the z-axis
790  REM  increment, plus one.
795  REM
800 ZZ = (2 * A(6) / A(9)) + 1
810 NM =  INT (ZZ + 0.1)
820  PRINT
830  PRINT "PROJECTED # OF X-AXIS DATA POINTS = ";XX
840  PRINT "PROJECTED # OF Y-AXIS DATA POINTS = ";YY
850  PRINT "TOTAL # OF PROJECTED DATA POINTS  = ";NM
860  PRINT "ACTUAL # OF DATA POINTS ON DISK   = ";DL / 2
870  PRINT
875  REM
880  REM  If the number of projected data points differs from the
890  REM  number of points stored on the diskette, the users is asked
900  REM  if he wants to alter the XX or YY variable.  If there is a
910  REM  discrepency, and it is not fixed, the resulting plot will
920  REM  be in error.
925  REM
930  IF DL / 2 = NM GOTO 990
940  PRINT BL$;"<<< DISCREPENCY >>>";BL$
950  INPUT "DO YOU WISH TO ALTER XX OR YY ? ";ANS$
960  IF  LEFT$ (ANS$,1) <  > "Y" THEN  GOTO 990
970  INPUT "ENTER # OF X DATA POINTS: ";XX
980  INPUT "ENTER # OF Y DATA POINTS: ";YY
990  INPUT "DO YOU WISH TO PLOT? (Y/N) ";ANS$
1000  IF  LEFT$ (ANS$,1) <  > "Y" THEN  STOP
1005  IF TS$ <  > "Y" THEN  PRINT BL$;"MUST USE LONGITUDINAL PLOT PROGRAM
     ": STOP
1010  GOSUB 13700
1020  PRINT D$;"PR#2"
```

```
1030 F1 = X3 / XX
1040 F2 = 1 - (X1 / F1)
1050  FOR Y = 0 TO 2 STEP (2 / (YY - 1))
1060 YX = X3 * Y / 13
1070 YZ = Z3 * Y / 5
1080 X = X1
1085 T1 = 1
1090  GOSUB 12700
1100  PRINT "PU", FN X(XP), FN Y(ZP),ET$
1110  FOR X = X1 TO (X2 + .01) STEP (X3 / (XX - 1))
1120  GOSUB 12700
1130  IF ZP > ZMAX((XP / F1) + F2 + .25) THEN  GOTO 1160
1140  PRINT "PU ", FN X(XP), FN Y(ZP),ET$
1150  GOTO 1180
1160 ZMAX((XP / F1) + F2) = ZP
1170  PRINT "PD", FN X(XP), FN Y(ZP),ET$
1180  NEXT X
1190  PRINT "PD", FN X(XP), FN Y(Z1 + YZ),ET$
1200  NEXT Y
1210  PRINT D$;"PR#3"
1215  PRINT "SAVE = ";"  ";SV
1220  STOP
12650  REM
12700  REM     ========================================================
12710  REM      This subroutine gets the next data point from memory.
12720  REM      ========================================================
12730  REM
12750  IF MB = 24576 THEN  GOSUB 30000
12800 A =  PEEK (MB)
12900 B =  PEEK (MB + 1)
12950  IF T1 <  > 0 THEN T1 = 0: GOTO 13100
13000 MB = MB + 2
13100 Z = (B * 16 + A) / 409.6
13200 XP = X + YX
13300 ZP = Z + YZ
13400  IF  ABS (ZP) < .01 THEN ZP = 0
13450 SV = MB
13500  RETURN
13600  REM
13700  REM   ============================================================
13701  REM    This subroutine sets up the HP-7470A plotter, then
13702  REM    draws and labels the axes.
13703  REM    ============================================================
13705  REM
13710 X1 = A(1) - A(4)
13720 X2 = A(1) + A(4)
13722 Y1 = A(2) - A(5)
13724 Y2 = A(2) + A(5)
13725  INPUT "Omit Labeling? (Y/N) ";LL$
13729 Z2 = 10
13730 Z1 = 0
13731  INPUT "ENTER MAXIMUM Z-AXIS VALUE: ";Z8
13732  INPUT "IS THIS IN WATTS OR mWatts? (W/M)";W$
13733  IF W$ = "W" THEN RN$ = "Watts": GOTO 13760
13734  IF W$ = "M" THEN RN$ = "mWatts": GOTO 13760
13735  GOTO 13732
```

```
13760 FS = 0
13770 MB = 16384
13780  INPUT "ENTER # OF X TICKS ->";XT
13790 ZT = 5
13795  IF LL$ = "Y" GOTO 15600
13800  PRINT "Enter first graph title line (within quotation marks)"
13900  INPUT T1$
13910  PRINT "Enter second graph title line"
13920  INPUT T2$
14000  PRINT D$;"PR#2"
14050  PRINT "IN;DF;SP 1";ET$
14100  PRINT "SC -1,1,-1,1";ET$
14200  PRINT "PU 0,.95",ET$
14300  PRINT "CP"; LEN (T1$) /  - 2;",0";ET$
14400  PRINT "LB ";T1$;ET$
14404  PRINT "PU 0,.90",ET$
14406  PRINT "CP"; LEN (T2$) /  - 2;",0";ET$
14408  PRINT "LB ";T2$;ET$
14410  PRINT "PA,-1 ,-.2",ET$
14420  PRINT "LBRECEIVED";ET$
14430  PRINT "CP;LBPOWER";ET$
14440  PRINT "CP;LB(";RN$;")";ET$
14450  PRINT "PA0,-.95";ET$
14460  PRINT "CP-10,0";ET$
14470  PRINT "LBX-AXIS POSITION (cm)";ET$
14480  PRINT "PA.75,-.5";ET$
14490  PRINT "LBY-AXIS";ET$
14500  PRINT "CP;LBPOSITION";ET$
14510  PRINT "CP;LB(cm)";ET$
15600 X3 = X2 - X1
15700 Z3 = Z2 - Z1
15710 XS = 10 ^ (3 -  INT ( LOG (X2 - X1)))
15720 YS = 10 ^ (3 -  INT ( LOG (Z2 - Z1)))
15800 S1 = (X1 - (1 / 3) * X3) * XS
15900 S2 = (X2 + (1 / 3) * X3) * XS
16000 S3 = (Z1 - (1 / 4) * Z3) * YS
16100 S4 = (Z2 + (1 / 2) * Z3) * YS
16110  DEF  FN X(X9) = X9 * XS
16120  DEF  FN Y(Y9) = Y9 * YS
16200  PRINT D$;"PR#2"
16300  PRINT "SP 1",ET$
16400  PRINT "SC ",S1,S2,S3,S4,ET$
16450  PRINT "PU", FN X(X1), FN Y(Z2),ET$
16500  PRINT "PD", FN X(X1), FN Y(Z1),ET$
16600  PRINT "PD", FN X(X2), FN Y(Z1),ET$
16700 X4 = (2 / 13) * X3
16800 Z4 = (2 / 5) * Z3
16900  PRINT "PD", FN X(X2 + X4), FN Y(Z1 + Z4),ET$
17000  PRINT "PU", FN X(X1), FN Y(Z1),ET$
17005  PRINT "PD", FN X(X1 + X4), FN Y(Z1 + Z4),ET$
17006  IF LL$ = "Y" GOTO 18900
17010  REM
17020  REM
17030  REM  Label the x-axis
17040  REM
17050  REM
```

```
17100  FOR X = X1 TO X2 + .01 STEP X3 / (XT - 1)
17200  IF  ABS (X) < .01 THEN X = 0
17300  PRINT "PU", FN X(X), FN Y(Z1),ET$
17400  PRINT "XT",ET$
17500 X$ =  LEFT$ ( STR$ (X),4)
17600  IF  ABS (X) < .01 THEN X$ = "0"
17700 LE =  LEN (X$) /  - 2
17800  PRINT "CP",LE;",-1.5;LB";X$;ET$
17810  NEXT X
17820  REM
17821  REM
17822  REM    Label the y-axis
17823  REM
17824  REM
17830  PRINT "PU", FN X(X2), FN Y(Z1),ET$
17840  PRINT "YT",ET$
17845 Y$ =  LEFT$ ( STR$ (Y1),4)
17847  IF  ABS (Y1) < .01 THEN Y$ = "0"
17850  PRINT "CP 1.75,-.25;LB";Y$;ET$
17855  PRINT "PU", FN X(X2 + X4), FN Y(Z1 + Z4),ET$
17860  PRINT "YT",ET$
17865 Y$ =  LEFT$ ( STR$ (Y2),4)
17870  IF  ABS (Y2) < .01 THEN Y$ = "0"
17875  PRINT "CP 1,-.25;LB";Y$;ET$
17910  REM
17920  REM
17930  REM  Label the z-axis
17940  REM
17950  REM
18000  FOR Z = 0 TO Z8 + .01 STEP Z8 / (ZT - 1)
18100  IF  ABS (Z) < .01 THEN Z = 0
18300  PRINT "PU", FN X(X1), FN Y(Z * Z2 / Z8),ET$
18400  PRINT "YT",ET$
18500 Z$ =  LEFT$ ( STR$ (Z),4)
18600  IF  ABS (Z) < .01 THEN Z$ = "0"
18700  PRINT "CP -4.5,-.25;LB";Z$;ET$
18800  NEXT Z
18900  PRINT D$;"PR#3"
18950  GOSUB 30000
19000  RETURN
30000  REM    ============================================================
30001  REM  This subroutine is called to load (BLOAD) the next 8K
30002  REM  file of scanner data into memory.
30003  REM  ============================================================
30200 D$ =  CHR$ (4)
30300  PRINT D$;"PR#3"
30310  VTAB 1: HTAB 1: PRINT " "
30320  VTAB 23: HTAB 30
30330  INVERSE
30400  PRINT "  LOADING DATA FILE ";F$;".";FS;"  ";
30450  NORMAL
30499 D$ =  CHR$ (13) +  CHR$ (4)
30500  PRINT D$;"BLOAD ";F$;".";FS;",A$4000"
30510  VTAB 23: HTAB 30: PRINT "                                    "
30750 FS = FS + 1
30760 MB = 16384
30770  PRINT D$;"PR#2"
30800  RETURN
```

REFERENCES

[1] J. G. Short, P. F. Turner, "Physical Hyperthermia and Cancer Therapy," Proc. IEEE, vol. 68, No. 1, pp. 133-142, 1980.

[2] J. F. Lehman, "Diathermy," Handbook for Physical Medicine and Rehabilitation, New York, NY, American Medical Association, pp. 273-345, 1971.

[3] C. C. Johnson, A. W. Guy, "Nonionizing Electromagnetic Wave Effects in Biological Materials and Systems," Proc. IEEE, vol. 60, no 6, pp. 692-620, 1972.

[4] C. A. Neyman, "Historical Development of Artificial Fever in the Treatment of Disease," New York, NY, Wiley, 1972.

[5] S. Licht, "History of Therapeutic Heat," Therapeutic Heat and Cold, Baltimore, MD, William and Wilkins, pp. 1-34, 1982.

[6] A. W. Guy, "Biophysics of High Frequency Currents and Electromagnetic Radiation," Therapeutic Heat and Cold, Baltimore, MD, William and Wilkins, pp. 199-277, 1982.

[7] L. S. Taylor, "Implantable Radiators for Cancer Therapy by Microwave Radiation," Proc. IEEE, vol. 68, no. 1, pp. 142-149, 1980.

[8] P. F. Turner, "Regional Hyperthermia with an Annular Phased Array," IEEE Trans. Biomed. Eng., vol. 31, no. 1, pp. 106-114, 1984.

[9] J. B. Anderson, "Theoretical Limitations on Radiation into Muscle Tissue," International Journal of Hyperthermia, vol. 1, no. 1, pp. 45-54, 1985.

[10] E. Gross, "Phased Array Microwave Heating at 915 MHz," Presented at IEEE MTT-S International Microwave Symposium, June 3, 1985.

[11] W. Gee, "Focusing Phased Array for Microwave Induced Hyperthermia Applications," Presented at IEEE MTT-S International Microwave Symposium, June 3, 1985.

[12] W. Gee, "Near Field Focusing Phased Array for Hyperthermia Application," Ph.D. Thesis, University of Illinois at Urbana-Champaign, Urbana, IL, 1983.

[13] Y. T. Lo, "An Improved Theory for Microstrip Antennas and Applications," IEEE Trans. Antennas Propagat., vol. 29, no. 1, pp. 38-46, 1981.

[14] R. Boesch, "Microwave Phase Shifter Design," EE 271 Term Paper, University of Illinois at Urbana-Champaign, Spring, 1985.

[15] D. Padgitt, "An Ultrasonic Transducer Field Scanner System," M.S. Thesis, University of Illinois at Urbana-Champaign, Urbana, IL, 1983.

[16] R. E. Shupe, "Heat Distribution in Phantom Studies," Hyperthermia and Cancer: Human Clinical Trial Experience, vol. 2, Boca Raton, FL, CRC Press, Inc., pp. 35-53, 1984.

[17] General Catalog, Engelmann Microwave Company, Whippany, NJ, p. 5, 1984.

[10] E. Gross, "Phased Array Microwave Heating at 915 MHz," Presented at IEEE MTT-S International Microwave Symposium, June 3, 1985.

[11] W. Gee, "Focusing Phased Array for Microwave Induced Hyperthermia Applications," Presented at IEEE MTT-S International Microwave Symposium, June 3, 1985.

[12] W. Gee, "Near Field Focusing Phased Array for Hyperthermia Application," Ph.D. Thesis, University of Illinois at Urbana-Champaign, Urbana, IL, 1983.

[13] Y. T. Lo, "An Improved Theory for Microstrip Antennas and Applications," IEEE Trans. Antennas Propagat., vol. 29, no. 1, pp. 38-46, 1981.

[14] R. Boesch, "Microwave Phase Shifter Design," EE 271 Term Paper, University of Illinois at Urbana-Champaign, Spring, 1985.

[15] D. Padgitt, "An Ultrasonic Transducer Field Scanner System," M.S. Thesis, University of Illinois at Urbana-Champaign, Urbana, IL, 1983.

[16] R. E. Shupe, "Heat Distribution in Phantom Studies," Hyperthermia and Cancer: Human Clinical Trial Experience, vol. 2, Boca Raton, FL, CRC Press, Inc., pp. 35-53, 1984.

[17] General Catalog, Engelmann Microwave Company, Whippany, NJ, p. 5, 1984.

UNIVERSITY OF ILLINOIS AT URBANA-CHAMPAIGN

THE GRADUATE COLLEGE

JULY 1985

WE HEREBY RECOMMEND THAT THE THESIS BY

TIMOTHY PAUL BENSON

ENTITLED THE DESIGN OF A MICROWAVE PHASED ARRAY HYPERTHERMIA SYSTEM

BE ACCEPTED IN PARTIAL FULFILLMENT OF THE REQUIREMENTS FOR

THE DEGREE OF MASTER OF SCIENCE

Director of Thesis Research

Head of Department

Committee on Final Examination†

Chairman

† Required for doctor's degree but not for master's.

O-517